Energy, Mines and Resources Canada
Énergie, Mines et Ressources Canada

CANMET

Canada Centre for Mineral and Energy Technology
Centre canadien de la technologie des minéraux et de l'énergie

Mining Research Laboratories
Laboratoires de recherche minière

HIGH TEMPERATURE UNIAXIAL AND TRIAXIAL COMPRESSION TESTS ON URL ROCK SAMPLES FROM BOREHOLE URL-05

J.S.O. Lau and B. Gorski

December 1990

Mining Research Laboratories
Divisional Report MRL 90-139(TR)

Canada

91-04786/

HIGH TEMPERATURE UNIAXIAL AND TRIAXIAL COMPRESSION TESTS ON URL ROCK SAMPLES FROM BOREHOLE URL-05

J.S.O. Lau and B. Gorski December 1990

Mining Research Laboratories
Divisional Report MRL 90-139(TR)

This document is the unedited
work prepared primarily
for [illegible] and internal
[illegible] It does not
represent final opinion of
the [illegible] of the Canada Centre
for Mineral and Energy Technology
(CANMET)

Ce document est le rapport
préliminaire non révisé et rédigé
principalement pour fin de
discussion et de documentation
interne. Il ne représente aucune
opinion finale ou définitive de
l'emploi du Centre canadien de
la technologie des minéraux et de
l'énergie (CANMET)

56 pp

MICROMEDIA

HIGH TEMPERATURE UNIAXIAL AND TRIAXIAL COMPRESSION TESTS ON URL ROCK SAMPLES FROM BOREHOLE URL-05

by

J.S.O. Lau[1] and B. Gorski[2]

ABSTRACT

A series of ambient room and high temperature uniaxial and triaxial compression tests were conducted on grey granitic core samples obtained from borehole URL-05 in the vicinity of the excavation of AECL Research's Underground Research Laboratory (URL). Twelve sets of tests were carried out at three temperatures (21° – 23°, 100° and 200° C) and four confining pressures (0, 3.5, 17 and 35 MPa) to study the thermo-mechanical properties of the grey granite.

The failure deviator stress and axial strain at failure were found to increase with increasing confining pressure. Heating up to 200° C reduced the failure deviator stress and the axial strain at failure.

The tangent Young's modulus and pseudo Young's modulus increased with increasing confining pressure at stress levels below approximately 60% of the failure deviator stress. Heating up to 200° C had some effects on these two moduli, reducing the mean modulus values by 5% to 8%.

The strength properties of the rock were expressed in terms of the Hoek and Brown failure criterion. When the temperature was raised from 21° – 23° to 100° and then to 200° C, the predicted uniaxial compressive strength of the intact rock material, σ_c, was found to decrease; and the material constant, m, was found to increase and then decrease. The Hoek and Brown failure envelopes derived from these tests show that the strength of the rock decreased with increasing temperature.

---

[1]Geotechnical Engineer, AECL Research, on attachment to Canadian Mine Technology Laboratory, Mining Research Laboratories, CANMET, Energy, Mines and Resources Canada, Ottawa, Ontario.

[2]Physical Scientist, Canadian Mine Technology Laboratory, Mining Research Laboratories, CANMET, Energy, Mines and Resources Canada, Ottawa, Ontario.

The Mohr-Coulomb friction angle, ϕ, decreased and the cohesive strength, c, increased with increasing confining pressure. Temperatures up to 200° C appeared to have no effect on ϕ. Under confined conditions, c decreased with increasing temperature.

Keywords: uniaxial, triaxial, compression, temperature, confining pressure, strength, strain, modulus, Hoek-Brown, Mohr-Coulomb

ESSAIS DE COMPRESSION UNIAXIALE ET TRIAXIALE À HAUTE TEMPÉRATURE SUR DES ÉCHANTILLONS DE ROCHE PROVENANT DU TROU DE SONDE URL-05

par

J.S.O. Lau[1] et B. Gorski[2]

RÉSUMÉ

Une série d'essais de compression uniaxiale et triaxiale à température ambiante et à haute température a été réalisée sur des échantillons carottés de roche granitique grise extraits du trou de sonde URL-05, au voisinage de l'excavation du Laboratoire de recherche souterraine (LRS) d'ÉACL Recherche. Douze séries d'essais ont été effectuées à trois températures (21° – 23°, 100° et 200° C) et sous quatre pressions de confinement (0, 3.5, 17 et 35 MPa) dans le but d'étudier les propriétés thermomécaniques du granite gris.

Nous avons observé que la contrainte déviatorique de rupture et la déformation axiale au moment de la rupture augmentaient lorsque la pression de confinement augmentait. Le chauffage à 200° C réduisait la constrainte déviatorique de rupture et la déformation axiale au moment de la rupture.

Le module tangent de Young et le pseudo module de Young augmentaient avec la pression de confinement à des niveaux de contrainte inférieurs à environ 60% de la contrainte déviatorique de rupture. Le chauffage à 200° C avait un certain effet sur ces deux modules, réduisant les valeurs moyennes de 5% à 8%.

Les caractéristiques de résistance de la roche ont été exprimées en fonction du critère de rupture de Hoek et Brown. Lorsque la température était élevée de 21° - 23° à 100°, puis à 200° C, la résistance à la compression uniaxiale prévue de la roche intacte,

---

[1]Ingénieur en géotechnique, EACL Recherche, affecté au Laboratoire canadien de technologie minière, Laboratories de recherche minière, CANMET, Énergie, Mines et Ressources Canada, Ottawa, Ontario.

[2]Chercheur en sciences physique, Laboratoire canadien de technologie minière, Laboratoires de recherche minière, CANMET, Énergie, Mines et Ressources Canada, Ottawa, Ontario.

σ_c, diminuait; la constante du matériau, m, aumentait d'abord, puis diminuait. Les enveloppes de rupture de Hoek et Brown établies à partir de ces essais montrent que la résistance de la roche diminuait lorsque la température augmentait.

L'angle de frottement de Mohr-Coulomb, ϕ, diminuait et la force de cohésion, c, augmentait lorsque la pression de confinement augmentait. Les températures inférieures à 200° C semblaient ne pas avoir d'effet sur ϕ. Dans des conditions de confinement, c diminuait lorsque la température augmentait.

Mots clés: uniaxiale, triaxiale, compression, température, pression de confinement, résistance, déformation, module, Hoek-Brown, Mohr-Coulomb

CONTENTS

	Page
ABSTRACT	i
RÉSUMÉ	iii
INTRODUCTION	1
SAMPLING AND SPECIMEN PREPARATION	2
DYNAMIC ELASTIC PROPERTIES	2
TEST APPARATUS AND PROCEDURE	3
TESTING PROGRAM	4
RESULTS AND DISCUSSION	4
Test Results	4
Failure Deviator Stress	5
Axial Strain at Failure	6
Tangent Young's Modulus	6
Pseudo Young's Modulus	7
Strength Properties	8
CONCLUSIONS	11
RECOMMENDATIONS	13
ACKNOWLEDGEMENTS	13
REFERENCES	14
APPENDIX A	37

TABLES

No.		
1.	Dimensions, densities and dynamic elastic properties of rock specimens.	15
2.	Results of ambient room and high temperature uniaxial and triaxial compression tests.	17
3.	Tangent Young's moduli at stress levels ranging from 10 to 90% of the failure deviator stress.	20
4.	Pseudo Young's moduli at stress levels ranging from 10 to 90% of the failure deviator stress.	22

5. Mean values and standard deviations (in brackets) of failure deviator stress, axial strains at failure, tangent Young's modulus, pseudo Young's modulus and Poisson's ratio. 24
6. Values of σ_c, m, s, r^2, σ_{cmass} and σ_{tmass} derived from the Hoek and Brown failure criterion. 25
7. Values of the Mohr-Coulomb friction angle ϕ and cohesive strength c. 26
8. Comparison of results from four series of tests. 27

FIGURES

1. Plots of failure deviator stress versus temperature. 29
2. Plots of axial strain at failure versus temperature. 30
3. Plots of mean tangent Young's modulus at the stress level of 50% of $(\sigma_1 - \sigma_3)_f$ versus temperature. 31
4. Plots of mean pseudo Young's modulus at the stress level of 50% of $(\sigma_1 - \sigma_3)_f$ versus temperature. 32
5. Hoek and Brown failure envelope for tests conducted at $21° - 23°$ C. 33
6. Hoek and Brown failure envelope for tests conducted at 100° C. 34
7. Hoek and Brown failure envelope for tests conducted at 200° C. 35
8. Effect of temperature on the Hoek and Brown failure envelope. 36

INTRODUCTION

As part of the Canadian Nuclear Fuel Waste Management Program (CNFWMP) concerned with the assessment of the feasibility and safety of the long-term disposal of high level nuclear wastes in vaults located at depth in plutonic rocks, AECL Research has constructed the Underground Research Laboratory (URL) in the Lac du Bonnet batholith in southeastern Manitoba. The URL allows the evaluation of characterization techniques and the assessment of modelling capabilities, and also provides a representative geological environment in which large-scale geotechnical and hydrogeological investigations can be conducted. In support of the geomechanical investigations at the URL, a high temperature uniaxial and triaxial testing program on URL core samples has been undertaken jointly by the Canada Centre for Mineral and Energy Technology (CANMET) and AECL Research. The purpose of the testing program is to establish the applicability of the thermo-mechanical rock properties measured on core samples in the laboratory for predicting the thermo-mechanical response of the rock mass surrounding the URL excavation. The information is also required for the development of the geotechnical data base for the URL characterization program.

Three series of uniaxial and triaxial compression tests at ambient room and high temperatures have been conducted on core samples of grey granite, obtained from the the 240 and 420 levels of the URL, and the results are presented in CANMET divisional reports MRL 90-5(TR) (Lau and Gorski, 1990a), MRL 90-079(TR) (Lau and Gorski, 1990b) and MRL 90-109(TR) (Lau and Gorski, 1990c). It should be noted that all samples used in those three series of tests were obtained in the URL during its construction phase. For the assessment of the disposal concept, it is important to demonstrate the ability to make accurate prediction of the thermo-mechanical properties of the rock on the basis of surface site evaluation, using core samples from surface-drilled boreholes. In order to find out whether such a prediction can be made, a similar series of uniaxial and triaxial tests have also been carried out for the URL characterization program on core samples from a surface-drilled borehole, URL-05, in the vicinity of the URL excavation. This report presents and discusses the test results from URL-05 core samples, and makes comparisons of these results with those obtained at the 240 and 420 levels of the URL.

SAMPLING AND SPECIMEN PREPARATION

Samples used in these tests were NQ rock cores obtained from borehole URL-05 between the downhole lengths of 269 and 294 m. The rock is a grey, medium- to coarse-grained granite, composed of approximately 30% K-feldspar, 30% plagioclase, 30% or slightly less quartz and 10% or slightly more mafic minerals, mainly biotite.

Specimens were prepared in accordance with the procedure described in the Pit Slope Manual Supplement 3-5 (Gyenge and Ladanyi, 1977) and the method suggested by the International Society for Rock Mechanics (Brown, 1981). The end surfaces of each of the specimens were ground flat to 0.025 mm to ensure that they were parallel to each other and perpendicular to the axis of the specimen. Table 1 shows the lengths, diameters and bulk densities of the specimens. It should be noted that in Table 1, the last number in the specimen identification represents the downhole length of the specimen. The mean bulk density of all the specimens was found to be 2.63 Mg/m^3. The specimen lengths varied from 98.68 to 114.96 mm and the diameters varied from 44.89 to 45.14 mm, with length to diameter ratios ranging from 2.2 to 2.5.

DYNAMIC ELASTIC PROPERTIES

Prior to the uniaxial and triaxial testing, compression (p) and shear (s) wave velocity measurements were made on the rock specimens. The purpose of the p- and s-wave measurements is to estimate various mechanical rock properties non-destructively prior to actual testing. The velocity measurements were made in accordance with the procedure described in the Pit Slope Manual Supplement 3-2 (Gyenge and Herget, 1977), using a pulse generator, pulsing and sensing heads and a Tektronix 2230 digital storage oscilloscope. The p- and s-wave velocities for each specimen were determined from their respective transit times along the longitudinal axis of the specimen. The dynamic elastic constants were computed from the measured wave velocities and the bulk density, using the following equations:

Dynamic Young' modulus of elasticity:

$$E_u = \frac{\rho V_s^2 (3V_p^2 - 4V_s^2)}{V_p^2 - V_s^2} \qquad (1)$$

where E_u = dynamic Young's modulus of elasticity
V_p = compression wave velocity
V_s = shear wave velocity
ρ = bulk density

Dynamic shear modulus:

$$G_u = \rho V_s^2 \tag{2}$$

where G_u = dynamic shear modulus

Dynamic Poisson's ratio:

$$\nu_u = \frac{V_p^2 - 2V_s^2}{2(V_p^2 - V_s^2)} \tag{3}$$

where ν_u = dynamic Poisson's ratio

The p-wave velocity, s-wave velocity, dynamic Young's modulus, dynamic shear modulus and dynamic Poisson's ratio determined for each of the specimens are given in Table 1. Table 1 also shows the mean values and standard deviations of the wave velocities and the dynamic elastic constants. The samples were found to have mean values of 4.030 km/s for p-wave velocity, 2.437 km/s for s-wave velocity, 37.84 GPa for dynamic Young's modulus, 15.67 GPa for dynamic shear modulus and 0.20 for dynamic Poisson's ratio. These values are lower than those determined for core samples from boreholes 209-021-SV1, 209-025-SV2, 209-030-DIL1 and 209-018-EXT4 located at the 240 level of the URL (Lau and Gorski, 1990b; Lau and Gorski, 1990c), but higher than those from borehole 401-009-HF1 located at the 420 level of the URL (Lau and Gorski, 1990a), suggesting that samples from URL-05 had more microcracks than those obtained at the 240 level, but less micrcracks than those obtained at the 420 level. This is not unexpected because the samples from URL-05 were obtained at depths between the 240 and 420 levels of the URL. The in situ stress and consequently the stress-induced microcracking due to unloading increase with depth at the URL (Martin, 1989), resulting in higher crack porosities for samples from greater depths.

TEST APPARATUS AND PROCEDURE

The uniaxial and triaxial compression tests were conducted using the MTS 815 Rock Mechanics Test System, a computer-controlled, servo-hydraulic compression machine, consisting of a 2.22 MN rated load cell, load frame, hydraulic power supply,

triaxial cell, test controller, test processor, temperature controller and DEC micro PDP 11/73 computer. The triaxial cell is rated up to 200° C and equipped with a heater, heat shroud, thermocouples, three linear variable differential transducers (LVDTs) for the measurement of axial strain and an extensometer with a circumferential kit for the measurement of circumferential strain. For a detailed description of the MTS system and its operation, the reader is referred to the MTS Operation Manual (MTS Systems Corp., 1986) and CANMET Division Report MRL 87-33(INT) (Gorski, 1987).

The uniaxial and triaxial test procedures have been described in CANMET divisional reports MRL 89-90(TR) (Lau and Gorski, 1989) and MRL 88-112(TR) (Lau et al., 1988) respectively, and therefore will not be repeated here. It should be noted that in the high temperature triaxial tests, specimens encapsulated in Teflon shrink tubing were heated to the test temperatures under confinement prior to the testing.

TESTING PROGRAM

Testing for this study took place between February and May, 1988 and in September, 1990 at Canadian Mine Technology Laboratory, Mining Research Laboratories, CANMET, Energy, Mines and Resources Canada in Ottawa. The testing program consisted of twelve sets of tests conducted under the unconfined condition and at the confining pressures of 3.5, 17 and 35 MPa and at the test temperatures of 21° – 23°, 100° and 200° C. The testing program is summarized in Table 2. A minimum of three tests were carried out in each set under the same confining pressure and temperature conditions in order to obtain statistically meaningful mean values. A total of 51 tests were performed for this study.

RESULTS AND DISCUSSION

TEST RESULTS

Table 2 summarizes the axial strain at failure, failure deviator stress, tangent Young's modulus and pseudo Young's modulus at the stress level equivalent to 50% of the failure deviator stress, Poisson's ratio, failure angle, θ, and failure characteristics of each of the specimens. It should be noted that results from three tests were rejected due to their incompatibility with the rest. The measurement of the axial strain was made using three LVDTs while the circumferential strain was measured using the bicycle chain

extensometer. Each axial strain, presented in Table 2 and illustrated in the stress-strain curve in Appendix A, is the average of the axial deformations obtained from the three LVDTs divided by the specimen length. The Poisson's ratio was determined as the ratio of the axial to the circumferential tangent moduli at the stress level equivalent to 50% of the failure deviator stress. It should be noted that no circumferential strain measurement was made in tests conducted in 1988, and thus, no Poisson's ratio was determined for those tests. The effects of the confining pressure and temperature on the strength and deformability of the rock samples will be discussed in the following subsections.

Stress versus strain curves for tests conducted in 1990 are presented in Appendix A of this report. Stress-strain curves for tests performed in 1988 are available in CANMET divisional report MRL 88-90(TR) and therefore will not be repeated in this report. These curves were plotted using DATAPLOT curve fitting computer software. A cubic spline fit was used for this analysis which employed a third degree equation model of the form:

$$\sigma = a_0 + a_1\varepsilon + a_2\varepsilon^2 + a_3\varepsilon^3 \qquad (4)$$

where σ = stress

ε = strain

and a_0, a_1, a_2 and a_3 are coefficients

FAILURE DEVIATOR STRESS

The failure deviator stresses of the specimens are shown in Table 2. Their mean values and standard deviations (in brackets) at different confining pressure and temperature conditions are given in Table 5. The failure deviator stresses and their mean values are also plotted against temperature in Figure 1. From these tables and plots, it can be seen that the failure deviator stress increased with the confining pressure at all test temperatures.

The effect of temperature on the failure deviator stress varied at different confining pressures. Under the unconfined condition and at the confining pressure of 35 MPa, temperature slightly influenced the failure deviator stress. The mean failure deviator stress increased by 2.3% as the temperature was increased to 100° C under the unconfined condition. However, when the temperature was further increased to 200° C, a net reduction of 3.9% was resulted. At the confining pressure of 35 MPa, the mean failure

deviator stress decreased by 0.6% and 5.0% as the temperature was raised to 100° and 200° C respectively. Temperature had considerable effect on the failure deviator stress at the confining pressures of 3.5 and 17 MPa. Reductions of the mean failure deviator stress at the temperatures of 100° and 200° C by as much as 20.9% and 21.7% respectively were observed at the confining pressure of 3.5 MPa, and by 10.1% and 13.9% respectively at the confining pressure of 17 MPa. These large reductions are attributed to the high failure deviator stresses obtained in tests performed at room temperature.

AXIAL STRAIN AT FAILURE

The axial strains at failure and their mean values at the four confining pressures and three test temperatures are given in Tables 2 and 5 respectively, and are also plotted versus temperature in Figure 2. They show that the axial strain at failure increased as the confining pressure increased.

Heating up to 200° C had some effect on the axial strain at failure. Under the unconfined condition, the mean axial strain at failure decreased by 7.3% when the temperature was raised to 100° C, but increased when the temperature was further raised to 200° C, reducing the decrease to only 2.5%. At the confining pressure of 3.5 MPa, significant reductions in the axial strain were observed as a result of heating. As the temperature was increased to 100° and 200° C, the mean axial strain at failure decreased by 19.9% and 13.3% respectively. The reductions at the confining pressure of 17 MPa were also high. Decreases of 7.7% and 10.3% were recorded at the temperatures of 100° and 200° C respectively. Temperature had less effect on the axial strain at the confining pressure of 35 MPa. Little change was observed at 100° C. Heating to 200° C reduced the mean axial strain at failure by only 3.6%.

TANGENT YOUNG'S MODULUS

Tangent Young's moduli for each of the rock specimens were computed from the stress-strain curve at nine stress levels equal to 10, 20, 30, 40, 50, 60, 70, 80 and 90% of the failure deviator stress, $(\sigma_1 - \sigma_3)_f$, and are presented in Table 3. The tangent moduli were determined by substituting the axial strain values corresponding to those nine stress levels into the derivatives of the best-fit equations (Equation 4) representing the stress-strain curve.

The tangent Young's modulus was found to vary at different stress levels. Under the unconfined condition, the tangent modulus increased until the deviator stress

reached a value equal to approximately 60% of $(\sigma_1 - \sigma_3)_f$, and then decreased until failure occurred. At the confining pressures of 3.5, 17 and 35 MPa, the tangent modulus behaved similarly, reaching the maximum values at stress levels equal to approximately 50%, 20-30% and 10-20% of $(\sigma_1 - \sigma_3)_f$ respectively.

The effect of confining pressure on the tangent modulus is considerable at stress levels below approximately 50% of $(\sigma_1 - \sigma_3)_f$. The tangent modulus at those stress levels increased as the confining pressure increased, especially at the onset of loading (low stress levels), suggesting that some stress relaxation had occurred in these specimens, resulting in higher crack porosities, larger deformations and lower modulus values at low confining pressures and low stress levels. This agrees with the results obtained from the measurements of wave velocities. At stress levels of 50-60% of $(\sigma_1 - \sigma_3)_f$, the modulus increased only when the confining pressure increased from 0 to 3.5 MPa (Fig. 3). At the stress levels above 60% of $(\sigma_1 - \sigma_3)_f$, the confining pressure appeared to have no effect on the tangent modulus.

The mean 50% (at the stress level equal to 50% of $(\sigma_1 - \sigma_3)_f$) tangent Young's moduli at different confining pressures and test temperatures are shown in Table 5. The mean 50% tangent moduli were also plotted against temperature in Figure 3. The modulus-temperature plots show that temperatures up to 200° C in general reduced the tangent modulus. The only exception was observed under the unconfined condition when the temperature was raised from room temperature to 100° C, where a 2.6% increase in the mean tangent modulus was recorded. The discrepancy is probably due to the variability of the rock. However, when the temperature was further raised to 200° C, a net reduction of 7.6% was noted. Under the confined conditions, the mean tangent modulus decreased with increasing temperature. As the temperature was increased to 100° and 200° C, the mean tangent modulus decreased by 4.9% and 6.6% respectively at the confining pressure of 3.5 MPa, by 5.1% and 5.5% respectively at the confining pressure of 17 MPa, and by 4.9% and 5.4% respectively at the confining pressure of 35 MPa.

PSEUDO YOUNG'S MODULUS

Actual stress versus axial strain curves for these specimens are nonlinear (see Appendix A). For modelling purposes, each nonlinear curve may be idealized as a series of straight lines joining points corresponding to stress levels of 0.0, 0.1, 0.2, 0.3, 0.4, 0.5, 0.6, 0.7, 0.8, 0.9 and 1.0 times the failure deviator stress. The slope of each of these straight lines is defined as the pseudo Young's modulus. The pseudo Young's moduli of the rock specimens are presented in Table 4. In general, the pseudo moduli are lower

than the tangent moduli at low stress levels, especially at low confining pressures, but higher than the tangent moduli at high stress levels.

The effects of confining pressure and temperature on the pseudo Young's modulus are similar to those on the tangent modulus. The pseudo modulus increased with increasing confining pressure only at stress levels below approximately 60% of $(\sigma_1 - \sigma_3)_f$. The mean 50% pseudo Young's moduli are shown in Table 5 and plotted against temperature in Figure 4. They show that heating up to 200° C had the same effect on the pseudo modulus as on the tangent modulus. Under the unconfined condition, the mean pseudo modulus increased by 2.7% when the temperature was raised to 100° C, and then decreased by 8.3% (from room temperature) as the temperature was further raised to 200° C. Under the confined conditon, as the temperature was increased to 100° C and then to 200° C, the mean Pseudo Young's modulus decreased by 4.8% and 7.6% respectively at the confining pressure of 3.5 MPa, by 4.5% and 5.5% respectively at the confining pressure of 17 MPa, and by 4.6% and 5.2% respectively at the confining pressure of 35 MPa.

STRENGTH PROPERTIES

The strength properties of the intact rock specimens can be expressed in terms of the Hoek and Brown failure criterion. The empirical relationship developed by Hoek and Brown (1980) between the principal stresses associated with the failure of a rock is given as follows:

$$\sigma_1 = \sigma_3 + \sqrt{m\sigma_c\sigma_3 + s{\sigma_c}^2} \tag{5}$$

where σ_1 = major principal stress at failure
σ_3 = minor principal stress applied to the rock sample
σ_c = uniaxial compressive strength of the intact rock material in the specimen
m and s are constants

According to the criterion, the values of m and s depend on the properties of the rock and the extent to which the rock has been broken before being subjected to the principal stresses σ_1 and σ_3. For these intact rock specimens, $s = 1$, and the uniaxial compressive strength of the intact rock material, σ_c, and the material constant, m, can be computed, using the following equations:

$$\sigma_c^2 = \frac{\sum y_i}{n} - \left[\frac{\sum x_i y_i - \frac{\sum x_i \sum y_i}{n}}{\sum x_i^2 - \frac{(\sum x_i)^2}{n}}\right]\frac{\sum x_i}{n} \tag{6}$$

$$m = \frac{1}{\sigma_c}\left[\frac{\sum x_i y_i - \frac{\sum x_i \sum y_i}{n}}{\sum x_i^2 - \frac{(\sum x_i)^2}{n}}\right] \tag{7}$$

where $x = \sigma_3$

$y = (\sigma_1 - \sigma_3)^2$

n = total number of data pairs x_i and y_i

The coefficient of determination r^2 is given by:

$$r^2 = \frac{\left[\sum x_i y_i - \frac{\sum x_i \sum y_i}{n}\right]^2}{\left[\sum x_i^2 - \frac{(\sum x_i)^2}{n}\right]\left[\sum y_i^2 - \frac{(\sum y_i)^2}{n}\right]} \tag{8}$$

The closer the value of r^2 is to 1.00, the better the fit between Equation 5 and the test data is.

Figures 5, 6 and 7 show the Hoek and Brown failure envelopes generated by using Equation 5 for tests conducted at the temperatures of 21° – 23°, 100° and 200° C respectively. The values of σ_c, m and r^2, computed by using Equations 6, 7 and 8, are presented in Table 6. The coefficient of determination, r^2, was found to range from 0.9639 to 0.9882, indicating that the fit of Equation 5 to the data was good.

The predicted uniaxial compressive strength of the intact rock material, σ_c, was found to decrease from 219 to 170 and then to 164 MPa when the temperature was raised from room temperature to 100° and then to 200° C. The decrease of σ_c from room temperature to 100° C is significantly high. The reason is that the predicted value of σ_c for specimens tested at room temperature is very high, and is also much higher than the uniaxial compressive strength (mean value = 188 MPa) actually obtained from the uniaxial compression tests (see Table 2). The Hoek and Brown failure envelope (Fig. 5) provides an explanation for this behaviour. The high predicted value for σ_c at room temperature is the result of the very high triaxial strengths observed at the confining

pressures of 3.5 and 17 MPa. These tend to raise the lower end of the failure envelope and ,in turn, significantly decrease the m value.

The m value was found to increase from 28.75 to 37.94 as the temperature was raised from room temperature to 100° C, and then decrease slightly to 36.18 as the temperature was raised to 200° C. The increase of the m value at 100° C is due to the very low value of m obtained at room temperature as explained above.

All three Hoek and Brown failure envelopes are plotted in Figure 9 to investigate the effect of temperature on the strength of the rock. They show some decrease in the strength of the rock with increasing temperature up to 200° C.

Hoek (1990) suggests that the uniaxial compressive strength of the rock mass, σ_{cmass}, can be computed by substituting $\sigma_3 = 0$ into Equation 5, yielding:

$$\sigma_{cmass} = \sqrt{s}\sigma_c \tag{9}$$

and the uniaxial tensile strength of the rock mass, σ_{tmass}, can be calculated by substituting $\sigma_1 = 0$ into Equation 5 and solving the resulting quadratic equation:

$$\sigma_{tmass} = \frac{\sigma_c}{2}(m - \sqrt{m^2 + 4s}) \tag{10}$$

The values of σ_{cmass} and σ_{tmass} derived from these tests, assuming $s = 1$, are also given in Table 6. It should be noted that under the in situ condition, the value of s is always less than one. Table 6 indicates that heating up to 200° C could lower both σ_{cmass} and σ_{tmass}.

Principal stress circles determined using the Hoek and Brown failure criterion can be used to generate the Mohr failure envelope from which the Mohr-Coulomb friction angle, ϕ, and the cohesive strength, c, can be measured (Hoek and Brown, 1980; Lau and Gorski, 1988). Hoek (1990) also suggests that the equivalent values for ϕ and c can be determined by using the following equations:

$$\sigma_n = \sigma_3 + \frac{(\sigma_1 - \sigma_3)^2}{2(\sigma_1 - \sigma_3) + \frac{1}{2}m\sigma_c} \tag{11}$$

where σ_n = normal stress

$$\tau = (\sigma_n - \sigma_3)\sqrt{1 + \frac{m\sigma_c}{2(\sigma_1 - \sigma_3)}} \tag{12}$$

where τ = shear stress

$$\phi = 90 - arcsin\left(\frac{2\tau}{\sigma_1 - \sigma_3}\right) \tag{13}$$

$$c = \tau - \sigma_n tan\phi \tag{14}$$

Mohr-Coulomb friction angles and cohesive strengths, computed by using Equations 11 to 14, are presented in Table 7. The friction angle was found to decrease while the cohesive strength increased with increasing confining pressure. Temperatures up to 200° C appeared to have no effect on ϕ. Under the confined conditions, c decreased with increasing temperature. However, c appeared not to be affected by temperature under the unconfined condition.

CONCLUSIONS

The results of these tests have provided some thermo-mechanical data as well as some insight into the behaviour of the core samples of grey granite obtained from the surface-drilled borehole, URL-05, in the vicinity of the URL excavation. The results also show that temperatures up to 200° C had some effects on the strength and deformability of the rock. Reductions in the failure deviator stress, axial strain at failure and modulus values were observed at 200° C. From the results, the following conclusions can be made.

The failure deviator stress increased as the confining pressure increased. Heating up to 200° C had considerable effect on the failure deviator stress at the confining pressures of 3.5 and 17 MPa, but little effect at the confining pressures of 0 and 35 MPa. When the temperature was raised from 21° – 23° to 100° C, the mean failure deviator stress increased by 2.3% under the unconfined condition, and decreased by 20.9%, 10.1% and 0.6% at the confining pressures of 3.5, 17 and 35 MPa respectively.

At the temperature of 200° C, reductions of 3.9%, 21.7%, 10.1% and 5.0% were recorded at the confining pressures of 0, 3.5, 17 and 35 MPa respectively. The large reductions at the confining pressures of 3.5 and 17 MPa are attributed to the high failure deviator stresses obtained in tests conducted at room temperature.

The axial strain at failure also increased with increasing confining pressure. Temperatures up to 200° C had some effect on the axial strain, especially at the confining pressures of 3.5 and 17 MPa. Heating up to 100° C decreased the mean axial strain at failure by 7.3%, 19.9% and 7.7% at the confining pressures of 0, 3.5 and 17 MPa respectively. At the high temperature of 200° C, reductions of 2.5%, 13.3%, 10.3% and 3.6% were observed at the confining pressures of 0, 3.5, 17 and 35 MPa respectively.

The tangent Young's modulus and pseudo Young's modulus increased as the confining pressure increased only at stress levels below approximately 60% of the failure deviator stress. The increase was particularly pronounced at low confining pressures and at low stress levels. At stress levels above 60% of the failure deviator stress, the confining pressure appeared to have no effect on the moduli.

Temperatures up to 200° C were found to have some effects on the tangent modulus and pseudo modulus. At the confining pressures of 3.5, 17 and 35 MPa, both moduli (at the stress level equal to 50% of $(\sigma_1 - \sigma_3)_f$) decreased by about 5% in mean values when the temperature was raised to 100° C. Under the unconfined condition, both moduli increased by approximately 3% in mean values. At the temperature of 200° C, the mean moduli decreased by 5% to 8% at all test confining pressures.

The strength properties of the rock specimens are expressed in terms of the Hoek and Brown failure criterion. The predicted uniaxial compressive strength of the intact rock material, σ_c, was found to decrease, and the material constant, m, was found to increase, and then decrease as the temperature was raised from $21° - 23°$ to 100° and then to 200° C. The Hoek and Brown failure envelopes derived from these tests show some decrease in the strength of the rock with increasing temperature up to 200° C.

Mohr-Coulomb friction angles and cohesive strengths of the rock were computed by using equations suggested by Hoek. The friction angle, ϕ, decreased and the cohesive strength, c, increased with increasing confining pressure. Temperatures up to 200° C appeared to have no effect on ϕ. The cohesive strength decreased with increasing temperature when tests were conducted under confined conditions.

To demonstrate the ability to make predictions of the thermo-mechanical properties of the grey granite surrounding the URL excavation, using core samples from a surface-drilled borehole in the vicinity of the URL excavation, results from four series

of uniaxial and triaxial compression tests at ambient room and high temperatures are compared in Table 8. Series 1 comprises tests on samples from boreholes 209-021-SV1 and 209-025-SV2, and series 2 on samples from boreholes 209-018-EXT4 and 209-030-DIL1 at the 240 level of the URL. Series 3 comprises tests on samples from borehole URL-05 presented in this report. Series 4 comprises tests on samples from borehole 401-009-HF1 at the 420 level of the URL. It can be seen from Table 8 that the failure deviator stresses and tangent Young's moduli obtained in series 3 compare favorably with those obtained from the other series.

RECOMMENDATIONS

One of the main rock mechanics issues related to the construction and operation of the URL is experimentally identifying the temperature-dependent strength and deformation characteristics of the host rock. This high temperature uniaxial and triaxial compression testing program on samples from a surface-drilled borehole has addressed this issue and is recommended for the URL characterization program during the operating phase of the URL and for any future site selection program if the disposal concept is deemed acceptable.

Ambient room temperature and high temperature tension tests should also be included in the testing program in order to obtain more accurate values of σ_c and m in the Hoek and Brown failure criterion.

Although results obtained from this testing program have shed some light on the thermo-mechanical properties of the URL rock samples, some questions remain to be answered. What are the scale effects on the thermo-mechanical properties of the URL rock samples? What are the effects of moisture on the thermo-mechanical properties? Will the rock behave the same way at very high confining pressure? These questions should be addressed in the future.

ACKNOWLEDGEMENTS

The authors wish to express their thanks to R. Jackson of CANMET for reviewing this report and making several helpful suggestions. Gratitude is expressed to J. Folta of CANMET for the preparation of specimens and for carrying out the compression wave and shear wave velocities measurements on the specimens.

REFERENCES

Brown, E.T. (1981), "Rock characterization testing and monitoring, ISRM suggested methods", International Society for Rock Mechanics, the Commission on Testing Methods, Pergamon, 211 p.

Gorski, B. (1987), "Post-failure uniaxial strength determinations using a servo-hydraulic test system", Division Report MRL 87-33(INT), CANMET, Energy, Mines and Resources Canada, 77 p.

Gyenge, M. and Herget, G. (1977), "Pit slope manual supplement 3-2 - laboratory tests for design parameters", CANMET, Report 77-26, 74 p.

Gyenge, M. and Ladanyi, B. (1977), "Pit slope manual supplement 3-5 - sampling and specimen preparation", CANMET, Report 77-29, 30 p.

Hoek, E. (1990), "Estimating Mohr-Coulomb friction and cohesion values from the Hoek-Brown failure criterion", Int. J. Rock Mech. Min. Sci. & Geomech. Abstr., Vol. 27, No. 3, p. 227-229.

Hoek, E. and Brown, E.T. (1980), "Underground excavations in rock", The institution of Mining and Metallurgy, London, 527 p.

Lau, J.S.O. and Gorski, B. (1990a), "High temperature uniaxial and triaxial compression tests on URL rock samples from borehole 401-009-HF1", Divisional Report MRL 90-5(TR), CANMET, Energy, Mines and Resources Canada, 90 p.

Lau, J.S.O. and Gorski, B. (1990b), "High temperature uniaxial and triaxial compression tests on URL rock samples from boreholes 209-021-SV1 and 209-025-SV2", Divisional Report MRL 90-079(TR), CANMET, Energy, Mines and Resources Canada, 46 p.

Lau, J.S.O. and Gorski, B. (1990c), "High temperature uniaxial and triaxial compression tests on URL rock samples from boreholes 209-018-EXT4 and 209-030-DIL1", Divisional Report MRL 90-109(TR), CANMET, Energy, Mines and Resources Canada, 62 p.

Martin, C.D. (1989), "Characterizing in situ stress domains at AECL's Underground Research Laboratory. Proceedings of the 42nd Canadian Geotechnical Conference, Winniprg, Manitoba, October 23-25, 1989, p. 61-74.

MTS Systems Corporation (1986), "Operation manual for 815 rock mechanics test systems", MTS Systems Corp., Minneapolis, Minnesota, U.S.A.

Table 1. Dimensions, densities and dynamic elastic properties of rock specimens.

Specimen identification	Length (mm)	Diameter (mm)	Bulk density (Mg/m^3)	P-wave velocity (km/s)	S-wave velocity (km/s)	Dynamic Young's modulus (GPa)	Dynamic shear modulus (GPa)	Dynamic Poisson's ratio
URL05-269.98	111.62	45.10	2.64	3.810	2.250	32.93	13.37	0.23
URL05-270.10	112.03	45.08	2.67	4.411	2.435	40.62	15.86	0.28
URL05-270.26	110.80	45.10	2.64	3.895	2.393	36.21	15.13	0.20
URL05-270.38	111.85	45.09	2.64	4.075	2.233	33.77	13.13	0.29
URL05-270.50	110.86	45.10	2.64	4.176	2.267	34.97	13.54	0.29
URL05-270.78	109.86	45.10	2.64	4.061	2.358	36.51	14.65	0.25
URL05-270.90	111.10	45.08	2.64	4.107	2.405	37.77	15.24	0.24
URL05-271.01	112.46	45.10	2.63	4.436	2.408	39.40	15.26	0.29
URL05-271.22	114.02	45.10	2.63	4.286	2.473	40.24	16.09	0.25
URL05-271.35	108.98	45.08	2.63	4.350	2.294	36.20	13.84	0.31
URL05-271.46	110.32	45.08	2.63	4.284	2.602	43.03	17.81	0.21
URL05-271.58	112.01	45.09	2.62	4.235	2.473	39.79	16.03	0.24
URL05-271.75	110.51	45.10	2.62	4.178	2.298	35.50	13.83	0.28
URL05-271.87	113.01	45.09	2.63	4.248	2.330	36.68	14.27	0.29
URL05-271.99	109.36	45.08	2.64	4.247	2.352	37.32	14.59	0.28
URL05-272.11	113.72	45.12	2.63	4.173	2.345	36.67	14.44	0.27
URL05-272.23	109.00	45.11	2.63	4.233	2.276	35.32	13.62	0.30
URL05-272.34	114.46	45.10	2.63	4.066	2.467	38.63	15.98	0.21
URL05-272.61	114.96	45.11	2.64	4.188	2.478	39.82	16.18	0.23
URL05-272.73	110.28	45.11	2.63	4.201	2.302	35.84	13.94	0.29
URL05-273.18	101.74	45.13	2.62	4.037	2.626	40.95	18.07	0.13
URL05-273.40	100.70	45.13	2.63	4.077	2.603	41.26	17.85	0.16
URL05-273.60	98.68	45.12	2.64	4.253	2.598	42.87	17.83	0.20
URL05-273.70	100.00	45.14	2.64	4.255	2.571	42.25	17.42	0.21
URL05-273.91	100.50	45.14	2.63	3.926	2.510	38.30	16.59	0.15
URL05-274.01	100.48	45.12	2.64	3.979	2.513	38.91	16.65	0.17
URL05-274.12	99.98	45.14	2.63	4.040	2.541	38.89	17.01	0.17
URL05-274.30	100.08	45.12	2.64	4.127	2.518	40.21	16.71	0.20
URL05-274.40	100.51	45.13	2.64	4.028	2.504	39.19	16.53	0.19
URL05-274.97	100.79	45.11	2.63	4.122	2.527	40.24	16.78	0.20
URL05-275.07	101.60	44.92	2.63	4.536	2.725	47.60	19.54	0.22
URL05-275.96	102.25	44.89	2.63	3.851	2.547	47.93	17.07	0.11
URL05-276.23	100.54	44.90	2.63	3.943	2.468	37.71	16.01	0.18
URL05-276.33	100.72	44.89	2.62	3.934	2.560	38.96	17.20	0.13
URL05-276.57	100.00	44.90	2.64	4.024	2.476	38.65	16.17	0.20
URL05-276.67	101.01	44.91	2.64	4.048	2.501	39.36	16.52	0.19
URL05-276.86	99.84	44.92	2.64	4.117	2.506	39.98	16.58	0.21
URL05-276.96	101.40	44.91	2.64	3.976	2.542	39.41	17.07	0.15
URL05-277.07	101.00	44.92	2.64	3.984	2.507	38.87	16.58	0.17
URL05-290.564	110.83	45.00	2.64	3.770	2.285	33.35	13.79	0.21
URL05-290.711	112.43	45.00	2.64	3.711	2.397	34.65	15.17	0.14
URL05-290.826	110.40	45.01	2.63	3.755	2.400	34.98	15.15	0.15

Table 1 - (Cont'd)

Specimen identification	Length (mm)	Diameter (mm)	Bulk density (Mg/m^3)	P-wave velocity (km/s)	S-wave velocity (km/s)	Dynamic Young's modulus (GPa)	Dynamic shear modulus (GPa)	Dynamic Poisson's ratio
URL05-290.940	109.74	45.00	2.64	3.598	2.375	33.18	14.90	0.11
URL05-291.284	109.91	45.00	2.64	3.982	2.521	39.11	16.78	0.17
URL05-292.389	114.45	45.01	2.62	3.704	2.275	32.47	13.56	0.20
URL05-292.600	112.11	44.98	2.63	3.616	2.207	30.83	12.81	0.20
URL05-292.715	108.42	45.00	2.63	3.700	2.393	34.36	15.07	0.14
URL05-292.828	108.76	45.03	2.63	3.737	2.401	34.83	15.16	0.15
URL05-292.943	107.87	45.02	2.63	3.694	2.397	34.35	15.11	0.14
URL05-293.058	109.36	45.03	2.63	3.670	2.388	33.98	14.99	0.13
URL05-293.286	111.45	45.03	2.64	3.678	2.444	34.84	15.77	0.10
Mean			2.63	4.030	2.437	37.84	15.67	0.20
Standard deviation			0.01	0.230	0.116	3.51	1.49	0.06

Table 2. Results of ambient and high temperature uniaxial and triaxial compression tests.

Specimen Identification	Confining Pressure (MPa)	Temp. (deg C.)	Total Axial Strain (%)	Failure Deviator Stress (MPa)	Tangent Young's Modulus (GPa)	Pseudo Young's Modulus (GPa)	Poisson's Ratio	θ (deg.)	Failure characteristics
URL05-292.389	0.0	21	0.398 0.372*	190	63.17 61.77*	62.49 61.23*	0.37 0.36*		multiple vertical cracks
URL05-292.600	0.0	21	0.395 0.377*	191	63.67 62.09*	62.90 61.43*	0.37 0.36*		multiple vertical cracks
URL05-292.715	0.0	21	0.396 0.393*	183	64.03 58.79*	62.91 58.31*	0.32 0.29*		multiple vertical cracks
URL05-290.564	0.0	100	0.367	201	66.88	66.19			multiple vertical cracks
URL05-291.284	0.0	100	0.369	195	64.49	63.69			multiple vertical cracks
URL05-293.058	0.0	100	0.365	181	64.49	63.49			multiple vertical cracks
URL05-290.826	0.0	200	0.406	187	59.71	58.46			multiple vertical cracks
URL05-292.943	0.0	200	0.372	168	55.41	54.16	0.28		multiple vertical cracks
URL05-290.940	1.7	200	0.379	187	61.23	60.12			multiple vertical cracks
URL05-271.87	3.5	23	0.477	272	69.20	69.37			multiple vertical cracks
URL05-271.99	3.5	23	0.492	274	68.51	68.82		69	2 fragments, shear fracture
URL05-290.711	3.5	21	0.495	271	68.50	68.93	0.33	70	3 fragments, fracture, wedge-shaped bottom end
URL05-269.98	3.5	100	0.391	204	64.67	64.34		70	3 fragments, shear fracture, conical top end
URL05-270.10†	3.5	100	0.344	176	65.55	65.27		57	2 fragments, curved fracture
URL05-273.18	3.5	100		220				70	2 fragments, shear fracture
URL05-273.40	3.5	100	0.376	220	66.83	67.56		75	2 fragments, shear fracture
URL05-273.60	3.5	100	0.407	217				72	3 fragments, shear fracture, bottom wedge
URL05-273.91	3.5	100	0.390	216	64.70	65.26		72	2 fragments, shear fracture

*computed from strain gauge measurements

†results rejected due to the incompatibility of the failure deviator stress with the rest

Table 2 - (Cont'd)

Specimen Identification	Confining Pressure (MPa)	Temp. (deg C.)	Total Axial Strain (%)	Failure Deviator Stress (MPa)	Tangent Young's Modulus (GPa)	Pseudo Young's Modulus (GPa)	Poisson's Ratio	θ (deg.)	Failure characteristics
URL05-270.90	3.5	200	0.463	229	62.79	62.43		75	3 fragments, shear fracture, wedge-shaped top end
URL05-271.01	3.5	200	0.440	228	64.85	64.42		68	2 fragments, shear fracture
URL05-273.70†	3.5	200		184				70	2 fragments, shear fracture
URL05-274.01	3.5	200	0.402	194	66.36	65.46		70	2 fragments, curved fracture
URL05-274.12†	3.5	200		167				69	2 fragments, curved fracture
URL05-275.96	3.5	200	0.386	202	62.88	62.95		72	2 fragments, shear fracture
URL05-272.11	17.0	23	0.717	434	70.07	71.40		72	2 fragments, curved fracture
URL05-272.23	17.0	23	0.712	418	68.97	70.32		70	2 fragments, shear fracture
URL05-292.828	17.0	21	0.669	391	68.69	69.86	0.39	70	2 fragments, fracture
URL05-270.26	17.0	100	0.614	368	68.79	69.80		70	2 fragments, shear frature
URL05-270.38	17.0	100	0.646	378	68.35	69.46		72	2 fragments, curved fracture
URL05-270.50	17.0	100	0.579	350	70.92	71.85		68	2 fragments, curved fracture
URL05-274.30	17.0	100	0.689	376	62.08	63.86		75	2 fragments, curved fracture
URL05-274.40	17.0	100	0.633	367	62.37	64.35		70	2 fragments, shear fracture
URL05-274.97	17.0	100	0.649	385	64.92	67.29		69	2 fragments, shear fracture
URL05-276.23	17.0	100	0.708	384	62.76	64.95		73	2 fragments, shear fracture
URL05-275.07	17.0	200	0.629	331	59.90	60.51		71	2 fragments, shear fracture
URL05-276.33	17.0	200		323				70	2 fragments, curved fracture

†results rejected due to the incompatibility of the failure deviator stress with the rest

Table 2 - (Cont'd)

Specimen Identification	Confining Pressure (MPa)	Temp. (deg C.)	Total Axial Strain (%)	Failure Deviator Stress (MPa)	Tangent Young's Modulus (GPa)	Pseudo Young's Modulus (GPa)	Poisson's Ratio	θ (deg.)	Failure characteristics
URL05-271.22	17.0	200	0.616	372	69.67	70.65		70	2 fragments, shear fracture
URL05-271.35	17.0	200	0.666	385				73	3 fragments, shear fracture, wedge-shaped bottom end
URL05-271.46	17.0	200	0.601	376	68.59	69.40		71	3 fragments, shear fracture, wedge-shaped top end
URL05-277.07	17.0	200	0.623	353	63.65	65.96		72	2 fragments, shear fracture
URL05-272.34	35.0	23	0.876	506				70	2 fragments, shear fracture
URL05-272.61	35.0	23	0.829	521	70.05	71.80		60	2 fragments, curved fracture
URL05-293.286	35.0	21	0.826	501	69.62	71.43	0.39	70	2 fragments, curved fracture
URL05-270.78	35.0	100	0.824	508	70.07	71.68		65	2 fragments,curved fracture, wedge-shaped bottom end
URL05-272.73	35.0	100	0.808	525	71.43	73.02		67	2 fragments, curved fracture
URL05-276.57	35.0	100	0.885	496	62.15	64.41		67	2 fragments, curved fracture
URL05-276.67	35.0	100	0.886	495	61.89	64.20		70	3 fragments,curved fracture, wedge-shaped top end
URL05-271.58	35.0	200	0.804	518	69.19	70.40		70	2 fragments, curved fracture
URL05-271.75	35.0	200	0.798	487	69.10	70.35		70	2 fragments, shear fracture
URL05-276.86	35.0	200	0.826	464	61.93	64.28		69	2 fragments, curved fracture
URL05-276.96	35.0	200	0.826	467	63.96	66.62		70	2 fragments, curved fracture

Table 3. Tangent Young's moduli at stress levels ranging from 10 to 90 % of the failure deviator stress.

Specimen Identification	σ_3 (MPa)	Temp. (deg C.)	Tangent Young's Modulus (GPa)								
			10 %	20 %	30 %	40 %	50 %	60 %	70 %	80 %	90 %
URL05-292.389	0.0	21	37.62	50.70	57.84	61.56	63.17	63.26	61.84	58.75	50.46
URL05-292.600	0.0	21	37.65	50.71	57.95	61.86	63.67	63.91	62.60	59.59	52.01
URL05-292.715	0.0	21	33.28	47.72	56.35	61.44	64.03	64.51	62.95	59.13	49.92
URL05-290.564	0.0	100	41.74	55.25	62.00	65.26	66.88	67.04	65.75	62.91	56.27
URL05-291.284	0.0	100	39.11	52.05	58.98	62.63	64.49	64.81	63.61	60.79	54.10
URL05-293.058	0.0	100	36.91	50.20	57.77	62.19	64.49	65.02	63.82	60.76	52.67
URL05-290.826	0.0	200	31.94	44.26	51.86	56.87	59.71	60.73	60.04	57.56	51.44
URL05-292.943	0.0	200	31.39	41.23	47.84	52.60	55.41	56.35	55.53	52.87	46.33
URL05-290.940	1.7	200	36.02	47.17	54.18	58.72	61.23	62.00	61.12	58.48	48.26
URL05-271.87	3.5	23	57.04	64.56	67.79	69.29	69.20				
URL05-271.99	3.5	23	57.90	65.63	67.98	68.91	68.51				
URL05-290.711	3.5	21	51.55	63.39	68.44	69.17	68.50	66.69	63.64	59.08	49.93
URL05-269.98	3.5	100	47.59	56.27	61.05	63.74	64.67				
URL05-273.40	3.5	100					66.83				
URL05-273.91	3.5	100					64.70				
URL05-270.90	3.5	200	44.71	53.38	58.77	61.76	62.79				
URL05-271.01	3.5	200	45.85	55.11	60.59	63.69	64.85				
URL05-274.01	3.5	200					66.36				
URL05-275.96	3.5	200					62.88				

Table 3 - (Cont'd)

Specimen Identification	σ_3 (MPa)	Temp. (deg C.)	Tangent Young's Modulus (GPa)								
			10 %	20 %	30 %	40 %	50 %	60 %	70 %	80 %	90 %
URL05-272.11	17.0	23	74.08	75.50	74.70	72.62	70.07				
URL05-272.23	17.0	23	72.85	74.43	73.34	71.55	68.97				
URL05-292.828	17.0	21	71.19	72.38	72.08	70.88	68.69	65.40	60.76	54.33	44.99
URL05-270.26	17.0	100	70.07	71.37	71.49	70.64	68.79				
URL05-270.38	17.0	100	70.93	71.88	71.58	70.42	68.35				
URL05-270.50	17.0	100	71.62	73.11	73.33	72.62	70.92				
URL05-274.30	17.0	100					62.08				
URL05-274.40	17.0	100					62.37				
URL05-274.97	17.0	100					64.92				
URL05-276.23	17.0	100					62.76				
URL05-275.07	17.0	200					59.90				
URL05-271.22	17.0	200	70.71	71.92	72.18	71.45	69.67				
URL05-271.46	17.0	200	69.86	70.62	70.75	70.08	68.59				
URL05-277.07	17.0	200					63.65				
URL05-272.61	35.0	23	80.21	79.04	76.46	73.49	70.05				
URL05-293.286	35.0	21	79.94	78.57	76.12	73.16	69.62	65.38	60.24	53.90	45.48
URL05-270.78	35.0	100	79.41	77.77	75.75	73.20	70.07				
URL05-272.73	35.0	100	80.94	79.20	77.11	74.54	71.43				
URL05-276.57	35.0	100					62.15				
URL05-276.67	35.0	100					61.89				
URL05-271.58	35.0	200	79.76	74.73	73.37	71.54	69.19				
URL05-271.75	35.0	200	73.35	74.36	73.23	71.50	69.10				
URL05-276.86	35.0	200					61.93				
URL05-276.96	35.0	200					63.96				

Table 4. Pseudo Young's moduli at stress levels ranging from 10 to 90 % of the failure deviator stress.

Specimen Identification	σ_3 (MPa)	Temp. (deg C.)	Pseudo Young's Modulus (GPa)								
			10 %	20 %	30 %	40 %	50 %	60 %	70 %	80 %	90 %
URL05-292.389	0.0	21	20.53	44.56	54.53	59.92	62.49	63.34	62.68	60.43	55.36
URL05-292.600	0.0	21	20.30	44.57	54.59	60.12	62.90	63.92	63.38	61.23	56.44
URL05-292.715	0.0	21	20.01	40.59	52.29	59.10	62.91	64.44	63.90	61.23	55.14
URL05-290.564	0.0	100	29.46	48.98	58.96	63.78	66.19	67.08	66.52	64.46	60.33
URL05-291.284	0.0	100	27.55	46.00	55.80	60.96	63.69	64.77	64.34	62.34	58.15
URL05-293.058	0.0	100	25.79	43.92	54.22	60.16	63.49	64.90	64.56	62.44	57.60
URL05-290.826	0.0	200	19.17	38.36	48.23	54.52	58.45	60.36	60.53	58.95	55.10
URL05-292.943	0.0	200	25.14	36.47	44.64	50.31	54.16	56.02	56.09	54.35	49.99
URL05-290.940	1.7	200	26.12	41.83	50.83	56.60	60.12	61.75	61.70	59.94	55.94
URL05-271.87	3.5	23	46.11	61.55	66.32	68.67	69.37				
URL05-271.99	3.5	23	39.77	62.89	66.92	68.56	68.82				
URL05-290.711	3.5	21	38.16	58.01	66.32	69.01	68.93	67.69	65.27	61.47	55.29
URL05-269.98	3.5	100	35.30	52.45	58.83	62.54	64.34				
URL05-273.40	3.5	100					67.56				
URL05-273.91	3.5	100					65.26				
URL05-270.90	3.5	200	39.69	49.18	56.26	60.43	62.43				
URL05-271.01	3.5	200	34.97	50.83	58.04	62.30	64.42				
URL05-274.01	3.5	200					65.46				
URL05-275.96	3.5	200					62.95				

Table 4 - (Cont'd)

Specimen Identification	σ_3 (MPa)	Temp. (deg C.)	Pseudo Young's Modulus (GPa)								
			10 %	20 %	30 %	40 %	50 %	60 %	70 %	80 %	90 %
URL05-272.11	17.0	23	62.23	75.54	75.01	73.57	71.40				
URL05-272.23	17.0	23	62.47	74.40	73.94	72.50	70.32				
URL05-292.828	17.0	21	59.33	72.11	72.31	71.56	69.86	67.13	63.18	57.66	49.88
URL05-270.26	17.0	100	66.98	70.88	71.51	71.15	69.80				
URL05-270.38	17.0	100	64.80	71.65	71.80	71.08	69.46				
URL05-270.50	17.0	100	65.10	72.57	73.30	73.05	71.85				
URL05-274.30	17.0	100					63.86				
URL05-274.40	17.0	100					64.35				
URL05-274.97	17.0	100					67.29				
URL05-276.23	17.0	100					64.95				
URL05-275.07	17.0	200					60.51				
URL05-271.22	17.0	200	70.52	71.37	72.13	71.90	70.65				
URL05-271.46	17.0	200	71.04	70.22	70.75	70.48	69.40				
URL05-277.07	17.0	200					65.96				
URL05-272.61	35.0	23	76.76	80.02	77.77	75.00	71.80				
URL05-293.286	35.0	21	73.41	79.56	77.38	74.68	71.43	67.54	62.86	57.13	49.88
URL05-270.78	35.0	100	80.25	78.60	76.79	74.51	71.68				
URL05-272.73	35.0	100	81.86	80.08	78.19	75.86	73.02				
URL05-276.57	35.0	100					64.41				
URL05-276.67	35.0	100					64.20				
URL05-271.58	35.0	200		75.85	74.08	72.49	70.40				
URL05-271.75	35.0	200	68.42	74.40	73.84	72.41	70.35				
URL05-276.86	35.0	200					64.28				
URL05-276.96	35.0	200					66.62				

Table 5. Mean values and standard deviations (in brackets) of failure deviator stress, axial strain at failure, tangent Young's modulus, pseudo Young's modulus and Poisson's ratio.

Confining pressure (MPa)	Temperature (° C)	Mean failure deviator stress (MPa)	Mean failure axial strain (%)	Mean tangent Young's modulus (GPa)	Mean Pseudo Young's modulus (GPa)	Mean Poisson's ratio
0.0	21	188.0 (4.4)	0.396 (0.002)	63.62 (0.43)	62.77 (0.24)	0.353 (0.029)
	100	192.3 (10.3)	0.367 (0.002)	65.29 (1.38)	64.46 (1.50)	
	200	180.7 (11.0)	0.386 (0.018)	58.78 (3.02)	57.58 (3.08)	
3.5	21-23	272.3 (1.5)	0.488 (0.010)	68.74 (0.40)	69.04 (0.29)	
	100	215.4 (6.6)	0.391 (0.013)	65.40 (1.24)	65.72 (1.66)	
	200	213.3 (17.9)	0.423 (0.035)	64.21 (1.73)	63.82 (1.38)	
17.0	21-23	414.3 (21.7)	0.699 (0.026)	69.24 (0.73)	70.53 (0.79)	
	100	372.6 (12.2)	0.645 (0.044)	65.74 (3.59)	67.37 (3.10)	
	200	356.7 (25.4)	0.627 (0.024)	65.45 (4.54)	66.63 (4.54)	
35.0	21-23	509.3 (10.4)	0.844 (0.028)	69.84 (0.30)	71.62 (0.26)	
	100	506.0 (14.0)	0.851 (0.041)	66.39 (5.07)	68.33 (4.68)	
	200	484.0 (24.9)	0.814 (0.015)	66.05 (3.67)	67.91 (3.00)	

Table 6. Values of σ_c, m, s, r^2, σ_{cmass} and σ_{tmass} derived from the Hoek and Brown failure criterion.

Test Temperature (°C.)	Number of specimens	σ_c (MPa)	m	s	r^2	σ_{cmass} (MPa)	σ_{tmass} (MPa)
21-23	12	219	28.75	1.00	0.9729	219	7.61
100	19	170	37.94	1.00	0.9882	170	4.48
200	17	164	36.18	1.00	0.9639	164	4.53

Table 7. Values of the Mohr-Coulomb friction angle ϕ and cohesive strength c.

Confining pressure (MPa)	Test temperature (°C)	Number of specimens	ϕ	c (MPa)
0.0	21	3	63°	22
	100	3	63°	23
	200	3	63°	22
3.5	21-23	3	59°	33
	100	5	62°	20
	200	4	61°	21
17.0	21-23	3	52°	49
	100	7	54°	36
	200	6	54°	35
35.0	21-23	3	49°	55
	100	4	50°	52
	200	4	49°	50

Table 8. Comparison of results from four series of tests.

Confining pressure (MPa)	Temperature (° C)	Mean failure deviator stress (MPa)				Mean tangent Young's modulus (GPa)			
		1	2	3	4	1	2	3	4
0.0	21-25	185.7 (3.5)	167.8 (6.6)	188.0 (4.4)	171.7 (4.0)	65.52 (1.12)	62.36 (2.43)	63.62 (0.43)	58.27 (1.23)
	75	186.0 (6.9)	166.0 (3.6)		169.3 (4.9)	66.24 (1.24)	63.09 (2.26)		58.55 (1.58)
	100			192.3 (10.3)				65.29 (1.38)	
	125	179.7 (2.5)	164.0 (3.6)		161.7 (2.1)	64.20 (0.46)	60.78 (3.36)		57.63 (1.93)
	200			180.7 (11.0)				58.78 (3.02)	
3.5	18-23	261.7 (5.9)	229.7 (8.7)	272.3 (1.5)	239.3 (5.5)	70.07 (0.85)	68.73 (0.14)	68.74 (0.40)	61.41 (0.90)
	75	263.0 (8.7)	233.3 (4.7)		234.3 (6.8)	72.88 (2.18)	72.14 (3.20)		61.32 (2.88)
	100			215.4 (6.6)				65.40 (1.24)	
	125	244.0 (3.5)	228.3 (9.2)		229.7 (6.7)	71.25 (1.50)	68.58 (1.22)		64.96 (2.32)
	200			213.3 (17.9)				64.21 (1.73)	
17.0	19-23	421.7 (8.1)	368.3 (4.0)	414.3 (21.7)	406.8 (7.6)	72.28 (1.11)	70.85 (1.42)	69.24 (0.73)	69.06 (1.50)
	75	403.3 (17.4)	368.3 (10.1)		407.0 (6.7)	71.16 (0.61)	69.46 (1.77)		68.96 (2.36)
	100			372.6 (12.2)				65.74 (3.59)	
	125	395.7 (5.5)	368.0 (10.1)		388.3 (21.6)	71.42 (1.65)	68.83 (2.40)		69.20 (2.20)
	200			356.7 (25.4)				65.45 (4.54)	

Series 1: boreholes 209-021-SV1 and 209-025-SV2
Series 2: boreholes 209-018-EXT4 and 209-030-DIL1
Series 3: borehole URL-05
Series 4: borehole 401-009-HF1

Table 8 - (Cont'd)

Confining pressure (MPa)	Temperature (° C)	Mean failure deviator stress (MPa)				Mean tangent Young's modulus (GPa)			
		1	2	3	4	1	2	3	4
35.0	21-23	543.0 (17.0)	497.0 (6.6)	509.3 (10.4)	542.7 (10.4)	70.98 (1.09)	71.27 (0.90)	69.84 (0.30)	69.68 (1.18)
	75	522.3 (16.6)	480.7 (6.4)		533.0 (8.7)	70.30 (1.10)	70.24 (0.52)		69.74 (1.71)
	100			506.0 (14.0)				66.39 (5.07)	
	125	513.0 (6.2)	490.7 (14.7)		523.0 (3.0)	71.18 (1.64)	71.38 (3.03)		69.01 (0.53)
	200			484.0 (24.9)				66.05 (3.67)	

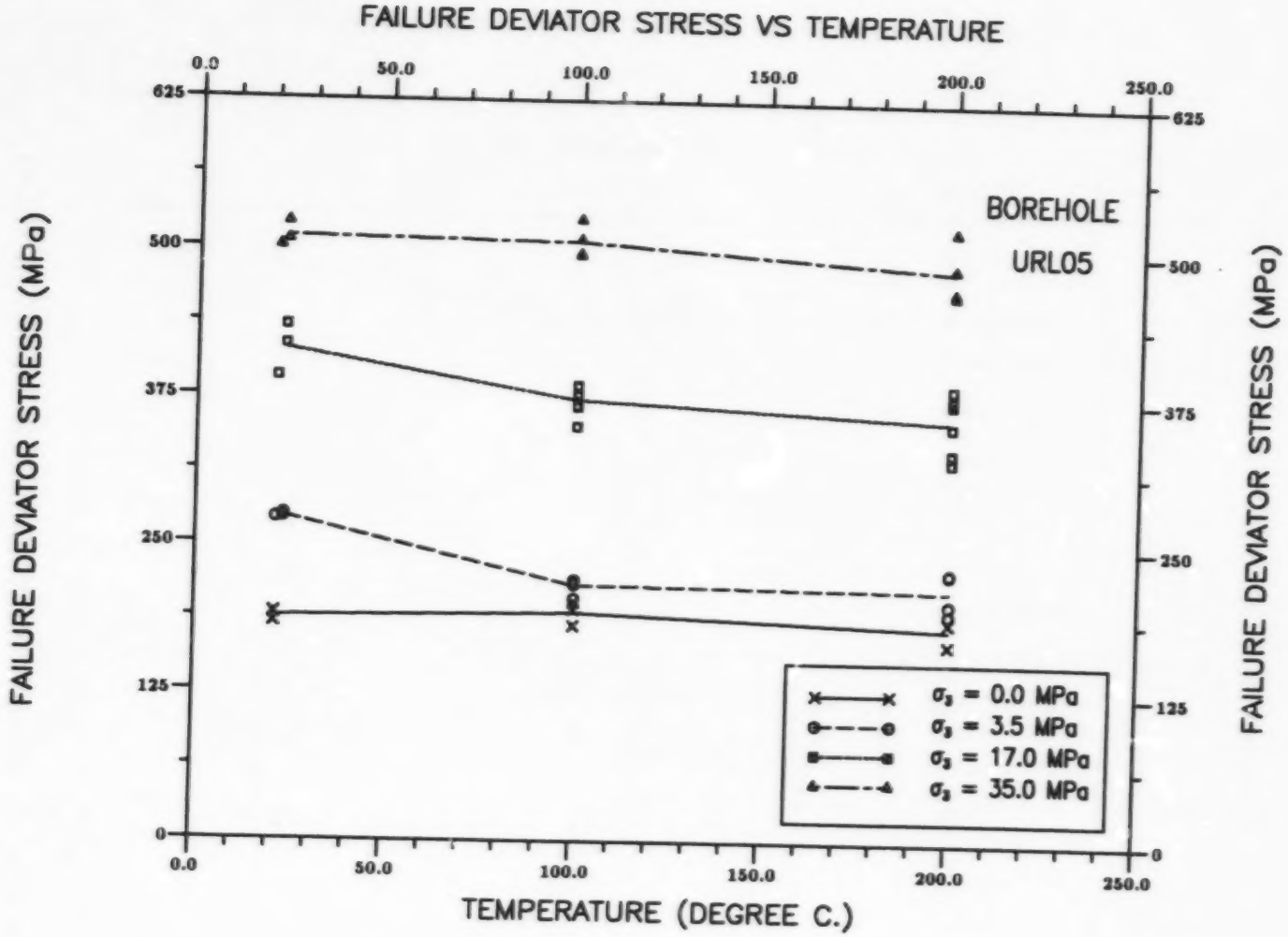

Figure 1. Plots of failure deviator stress versus temperature.

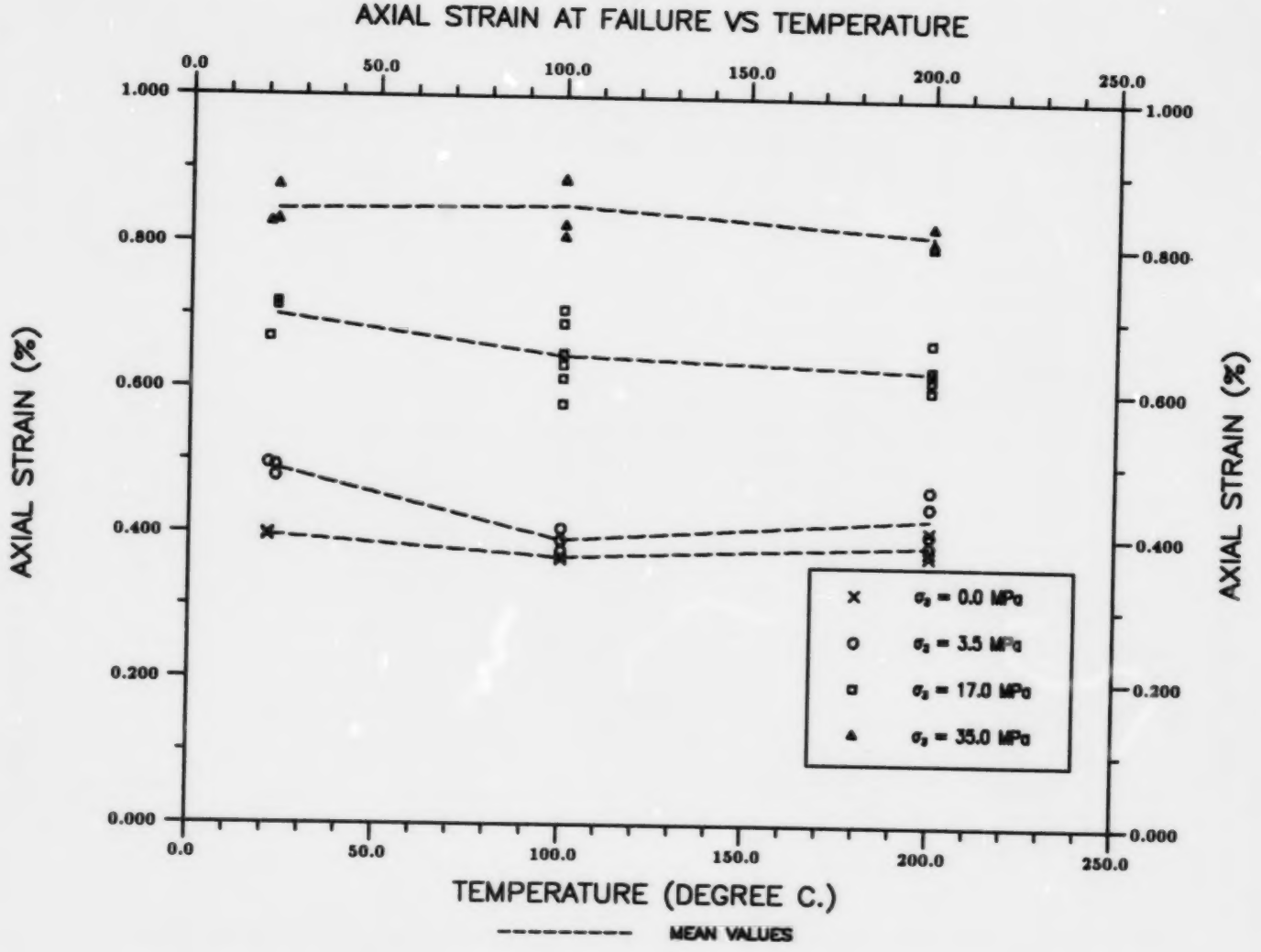

Figure 2. Plots of axial strain at failure versus temperature.

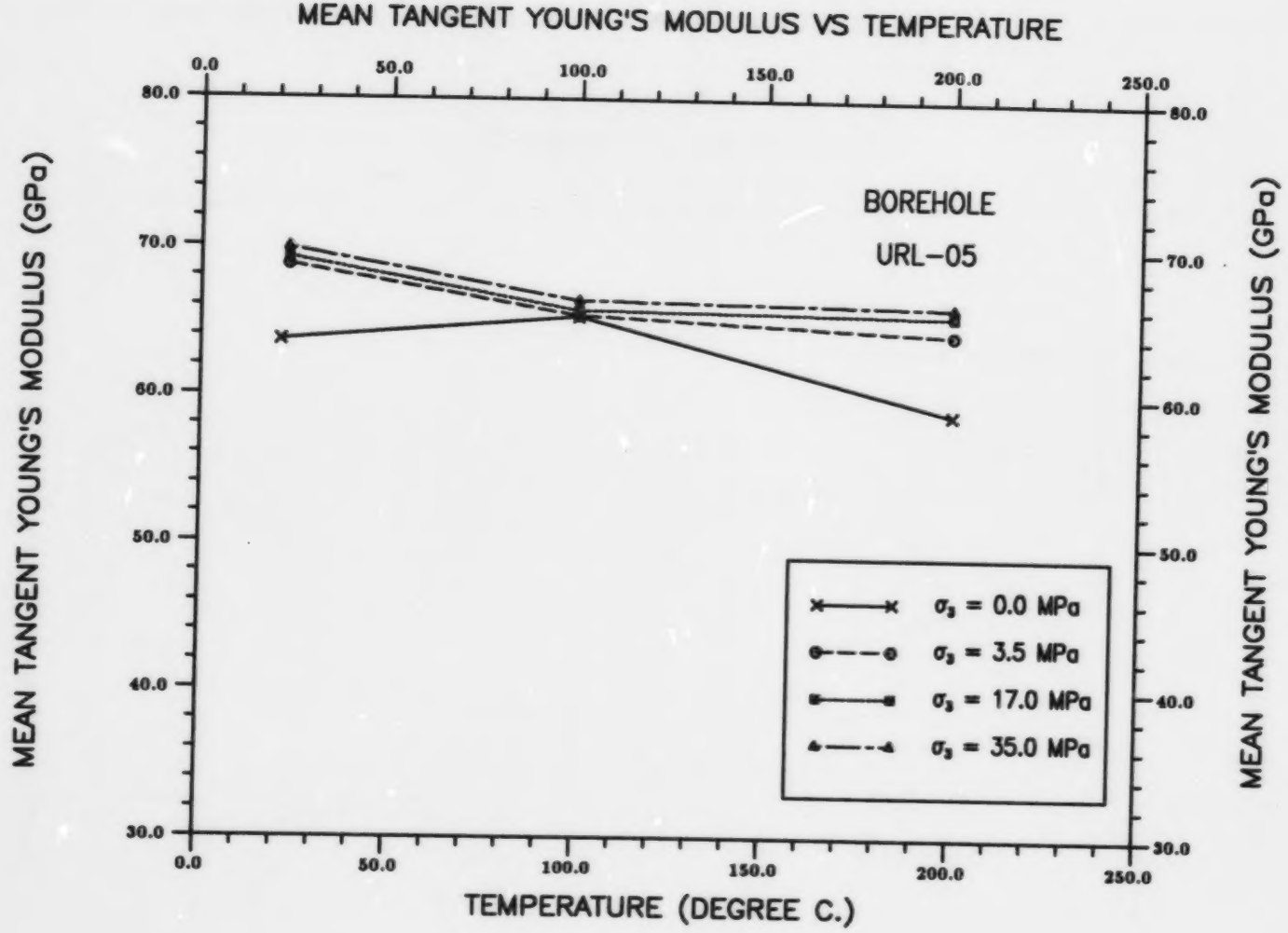

Figure 3. Plots of mean tangent Young's modulus at the stress level of 50 % of $(\sigma_1 - \sigma_3)_f$ versus temperature.

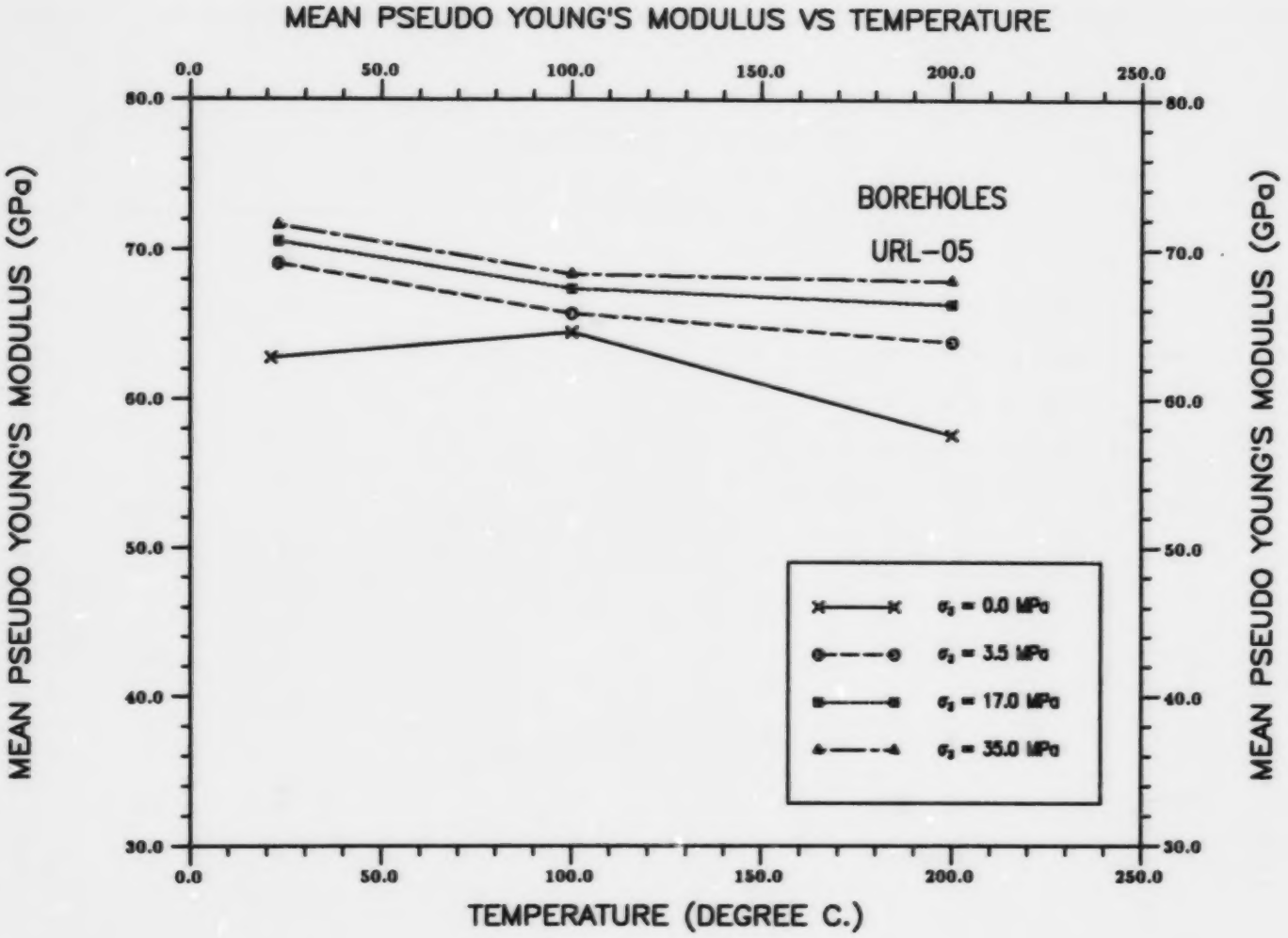

Figure 4. Plots of mean pseudo Young's modulus at the stress level of 50 % of $(\sigma_1 - \sigma_3)_f$ versus temperature.

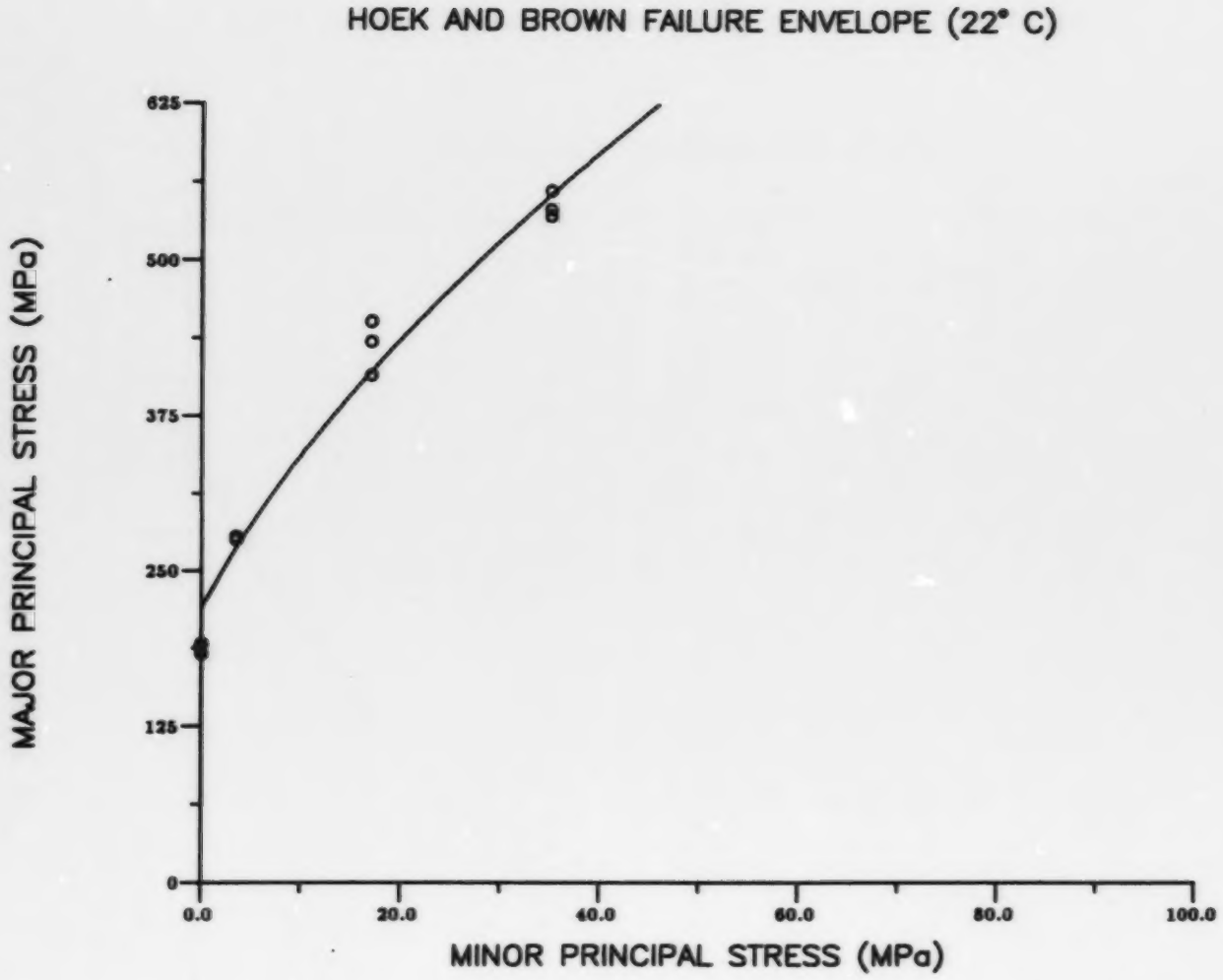

Figure 5. Hoek and Brown failure envelope for tests conducted at 21° – 23° C.

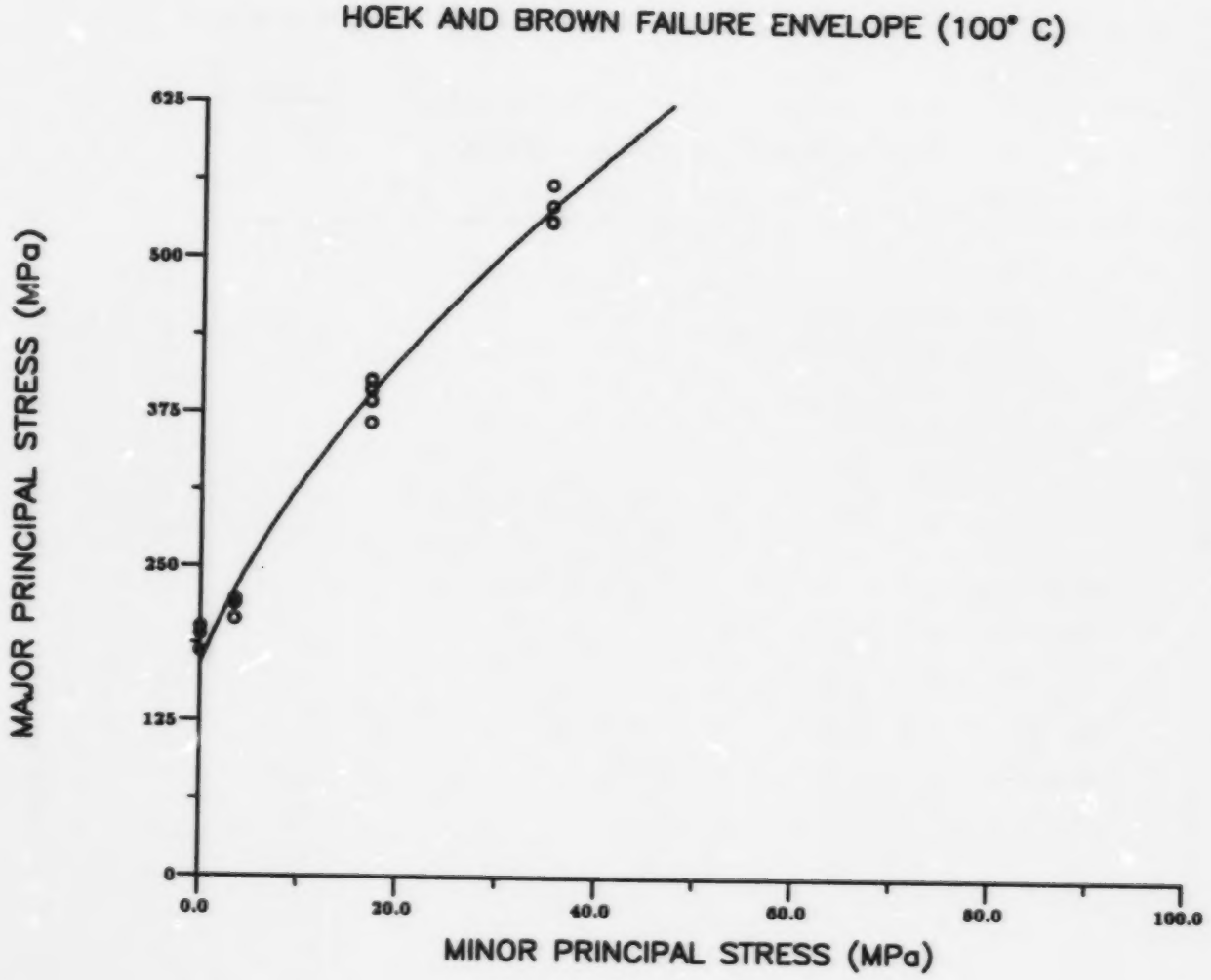

Figure 6. Hoek and Brown failure envelope for tests conducted at 100° C.

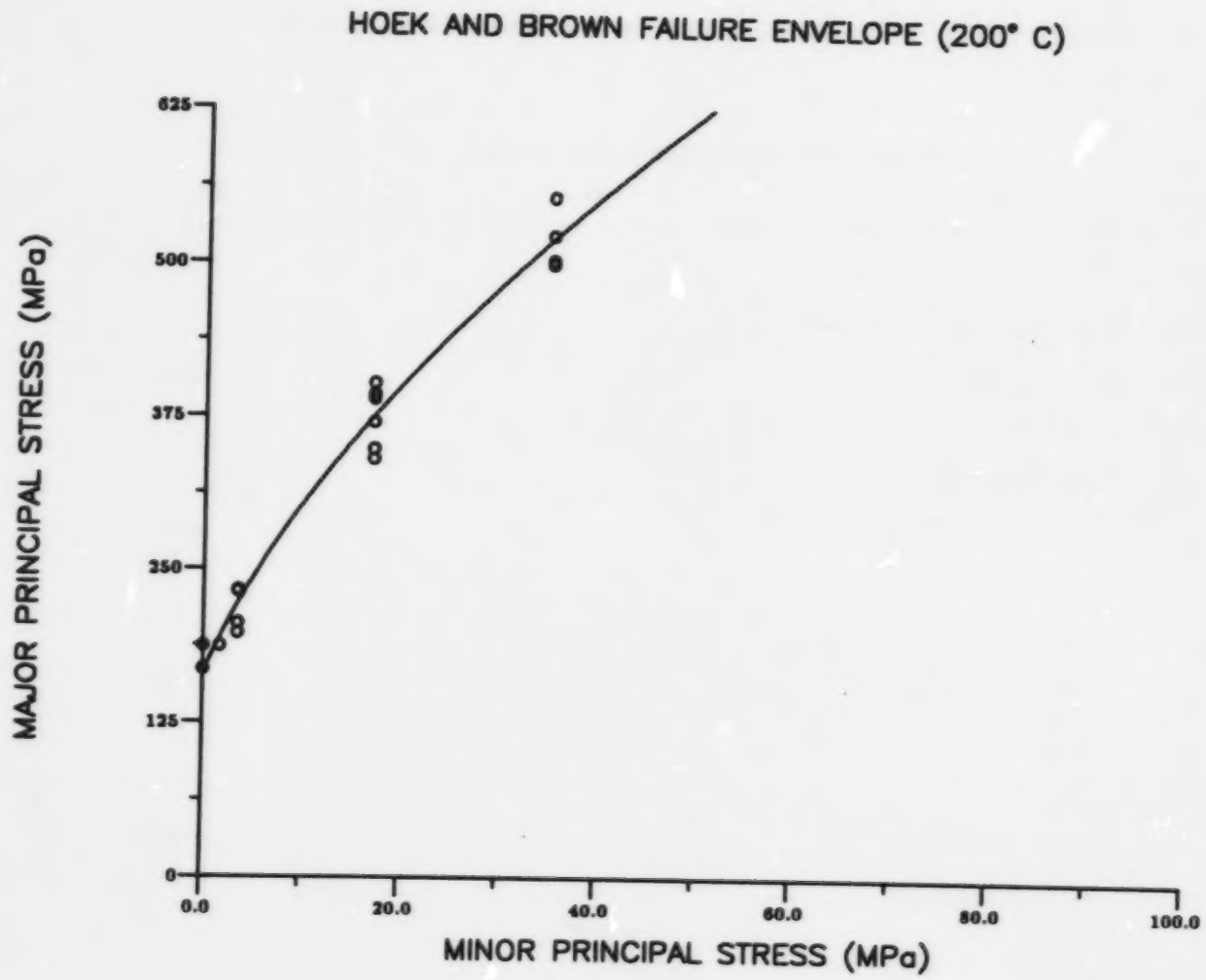

Figure 7. Hoek and Brown failure envelope for tests conducted at 200° C.

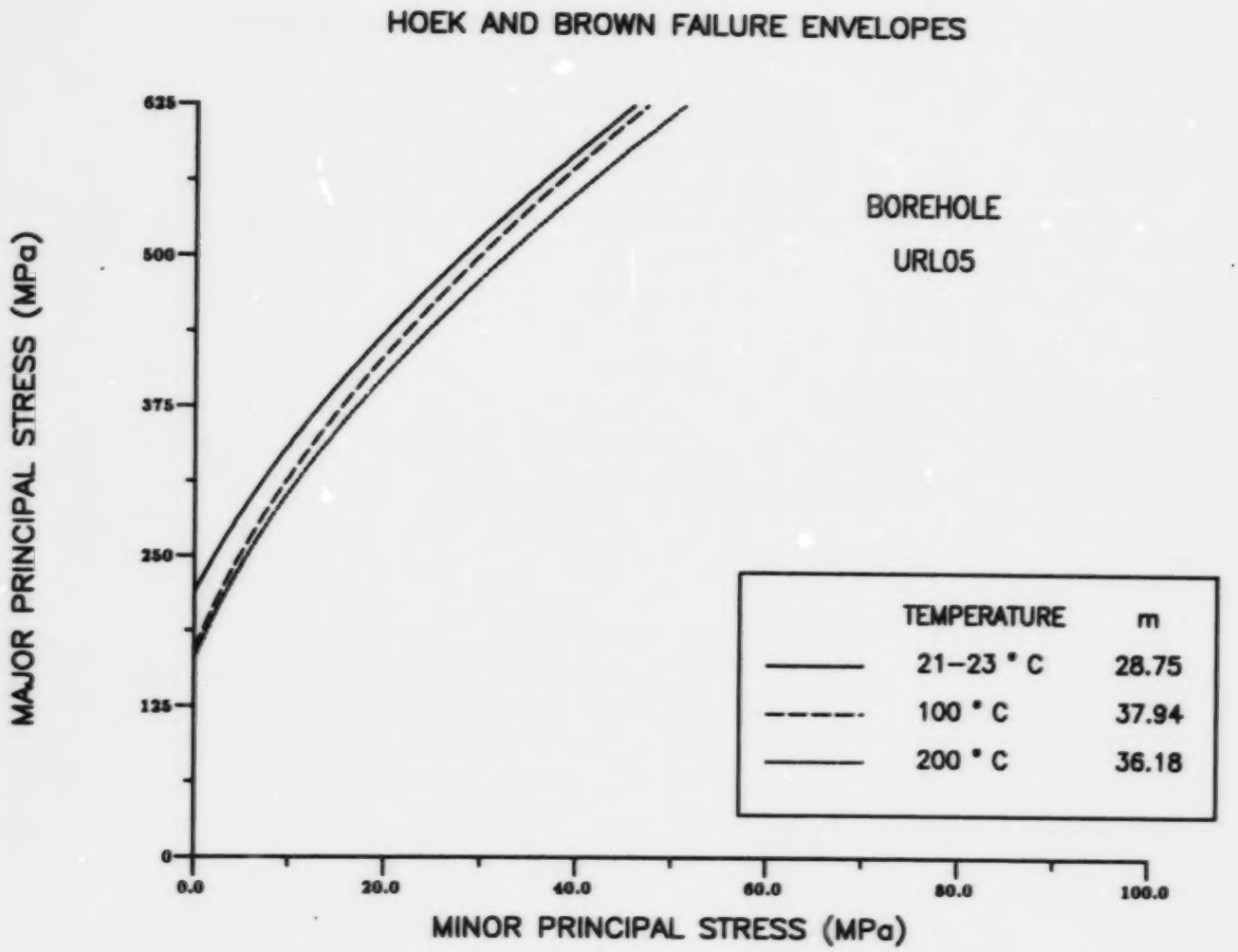

Figure 8. Effect of temperature on the Hoek and Brown failure envelope.

APPENDIX A

Stress-strain Curves

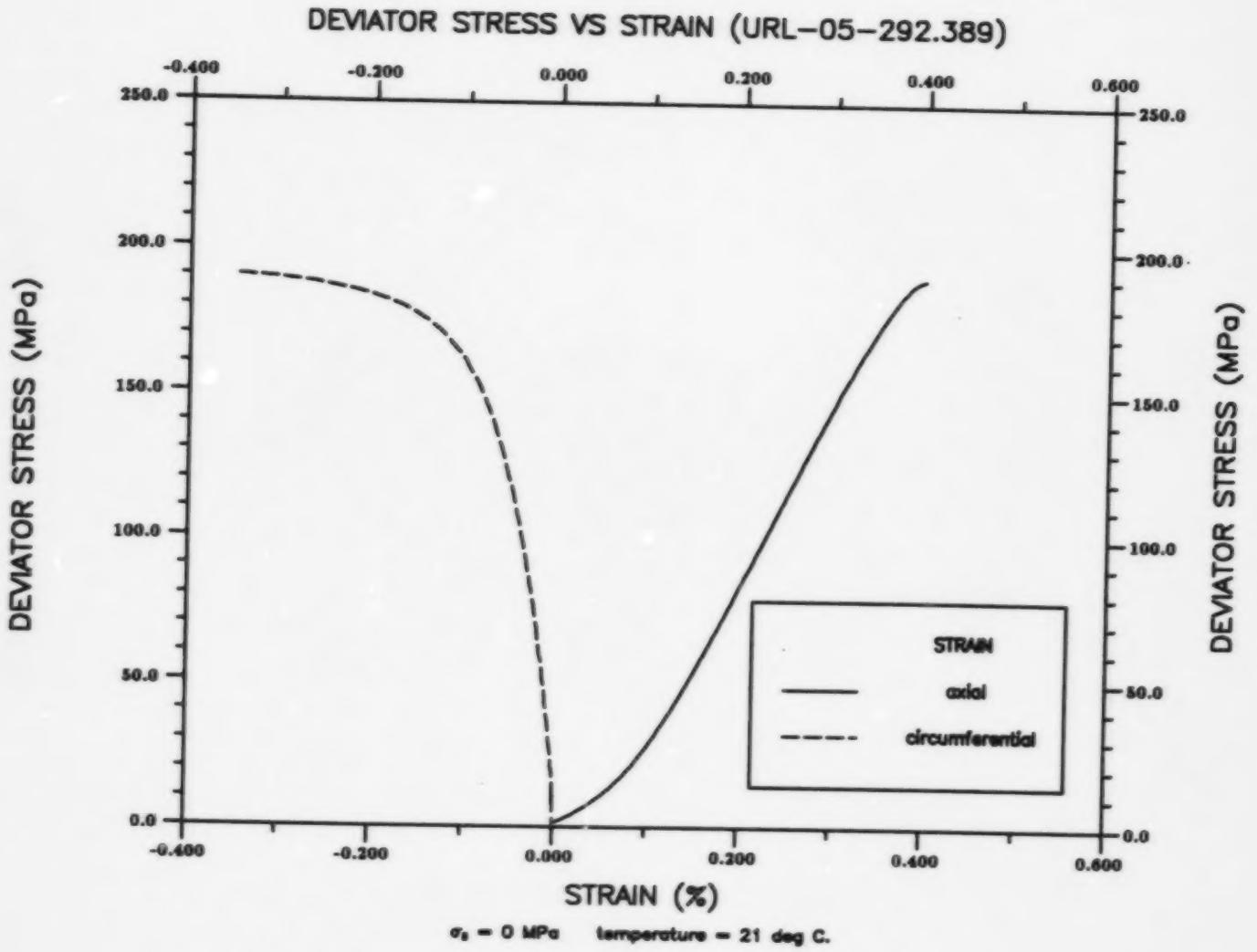

Figure A1. Stress-strain curves for Specimen URL05-292.389 tested at 21° C under the unconfined condition.

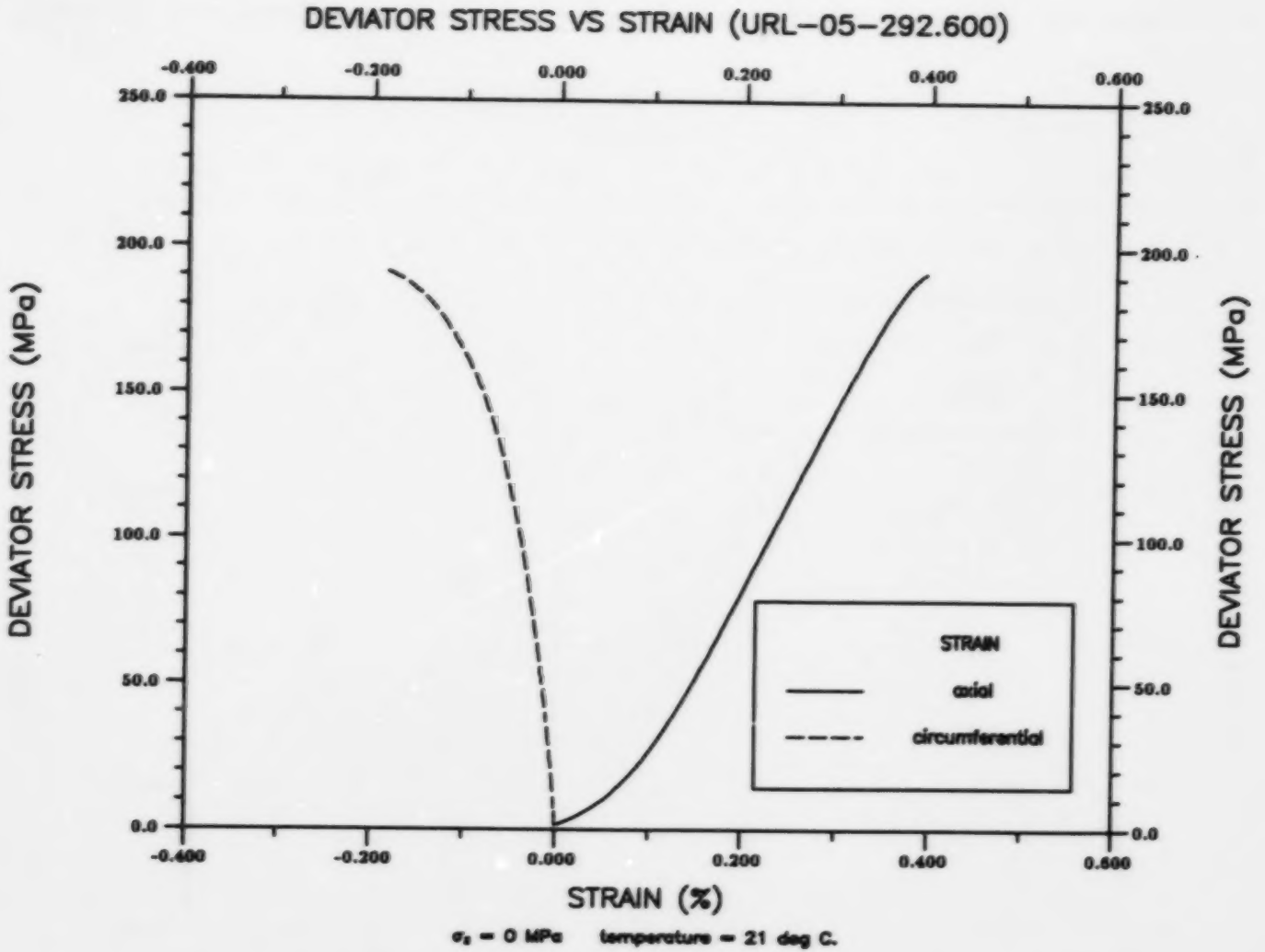

Figure A2. Stress-strain curves for Specimen URL05-292.600 tested at 21° C under the unconfined condition.

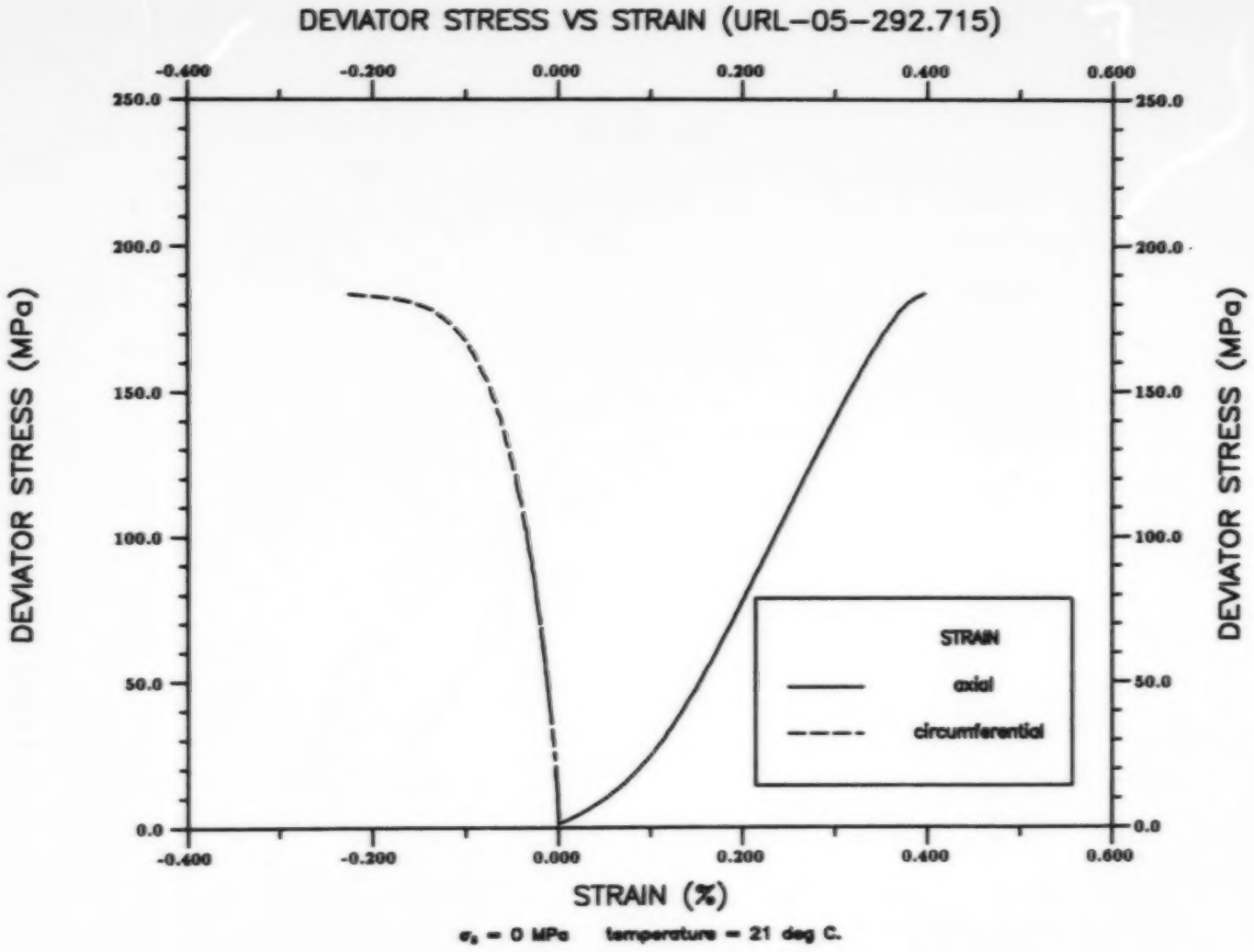

Figure A3. Stress-strain curves for Specimen URL05-292.715 tested at 21° C under the unconfined condition.

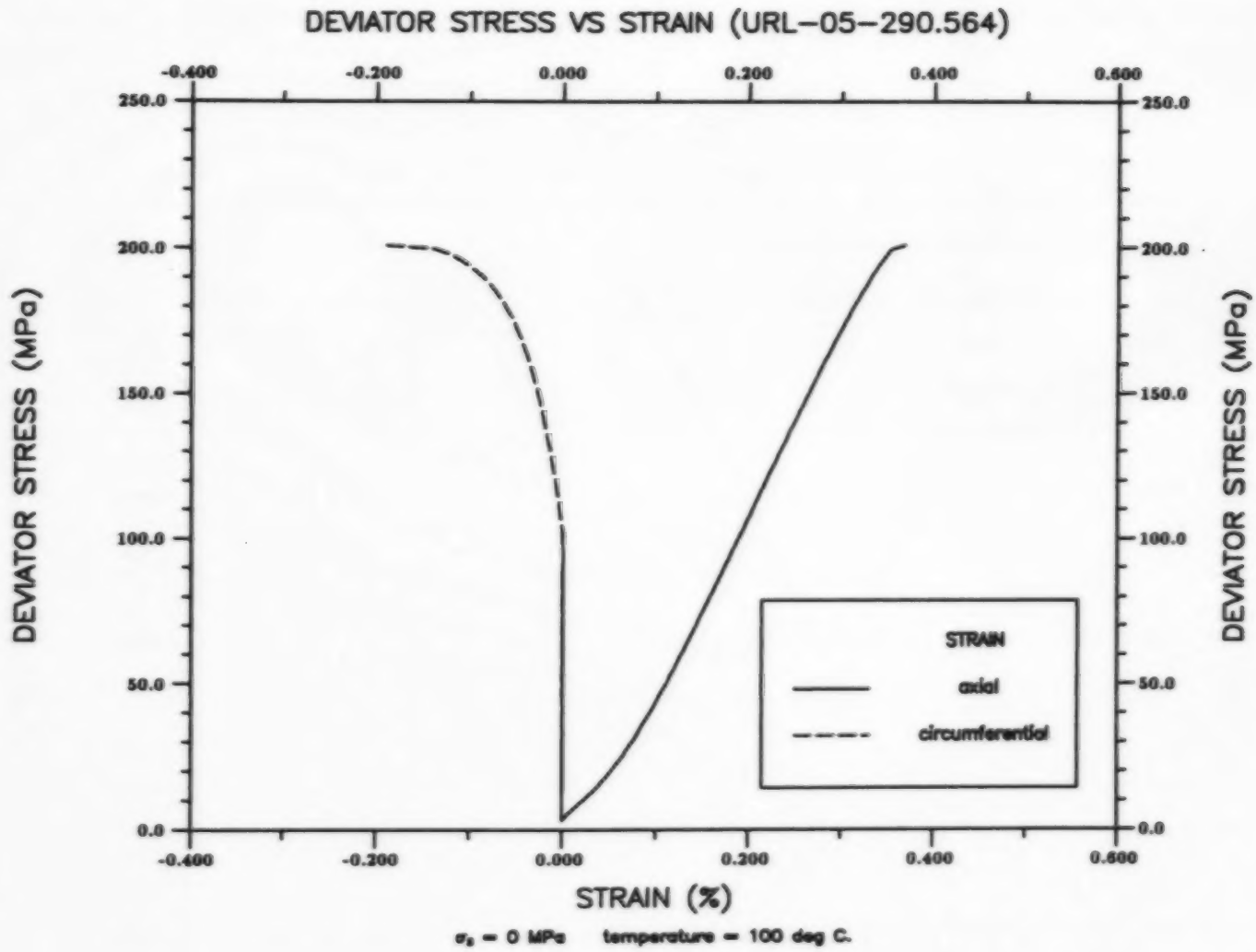

Figure A4. Stress-strain curves for Specimen URL05-290.564 tested at 100° C under the unconfined condition.

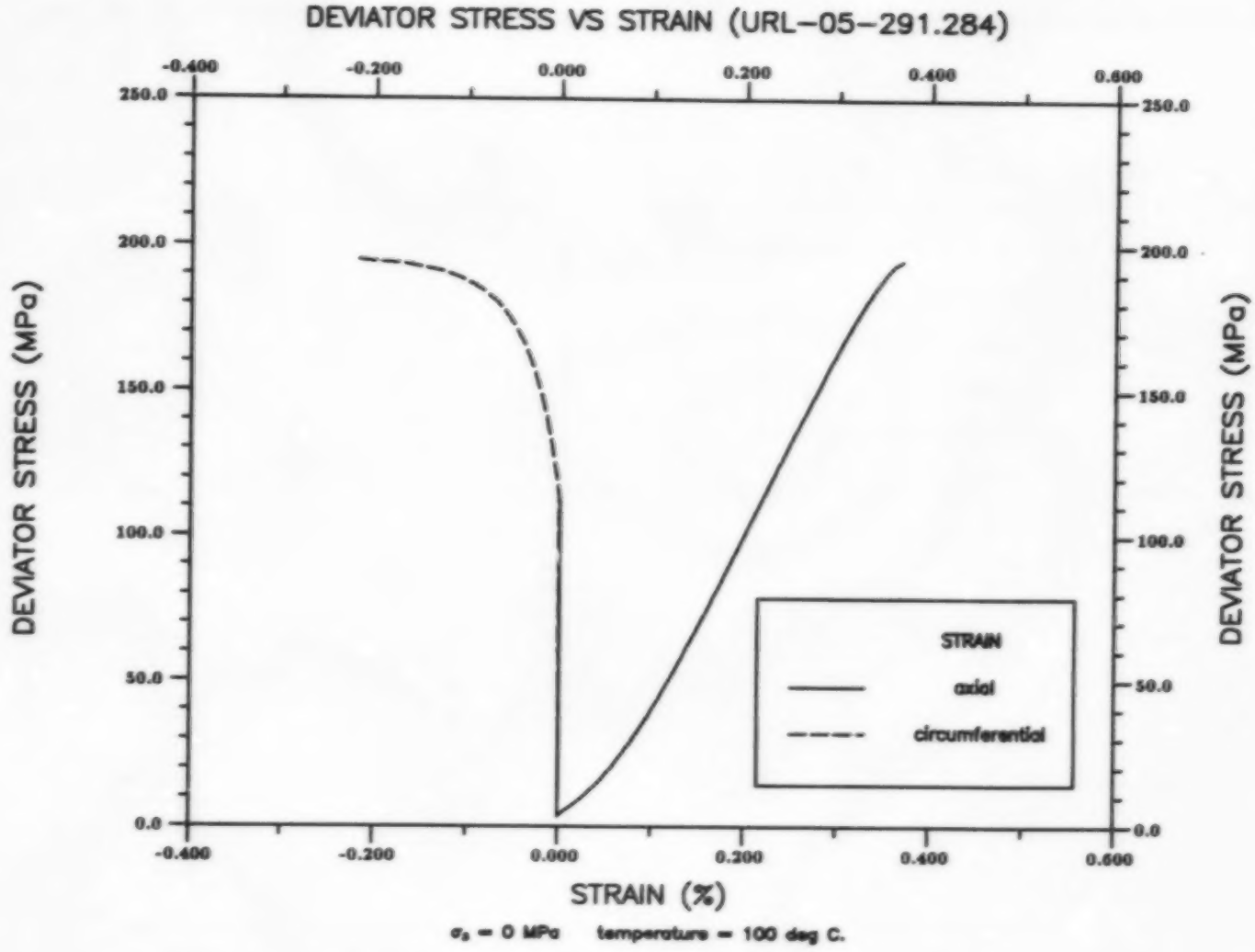

Figure A5. Stress-strain curves for Specimen URL05-291.284 tested at 100° C under the unconfined condition.

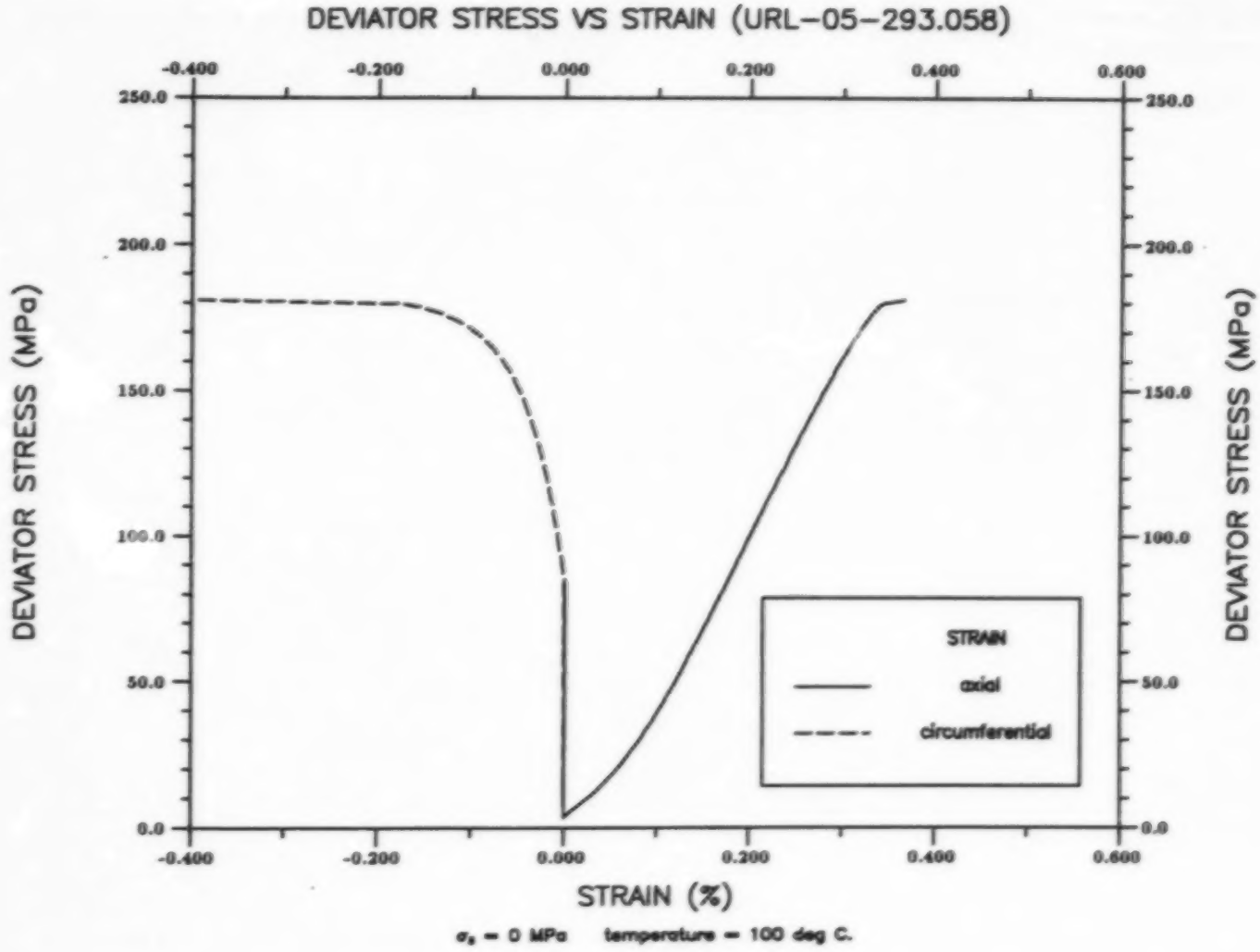

Figure A6. Stress-strain curves for Specimen URL05-293.058 tested at 100° C under the unconfined condition.

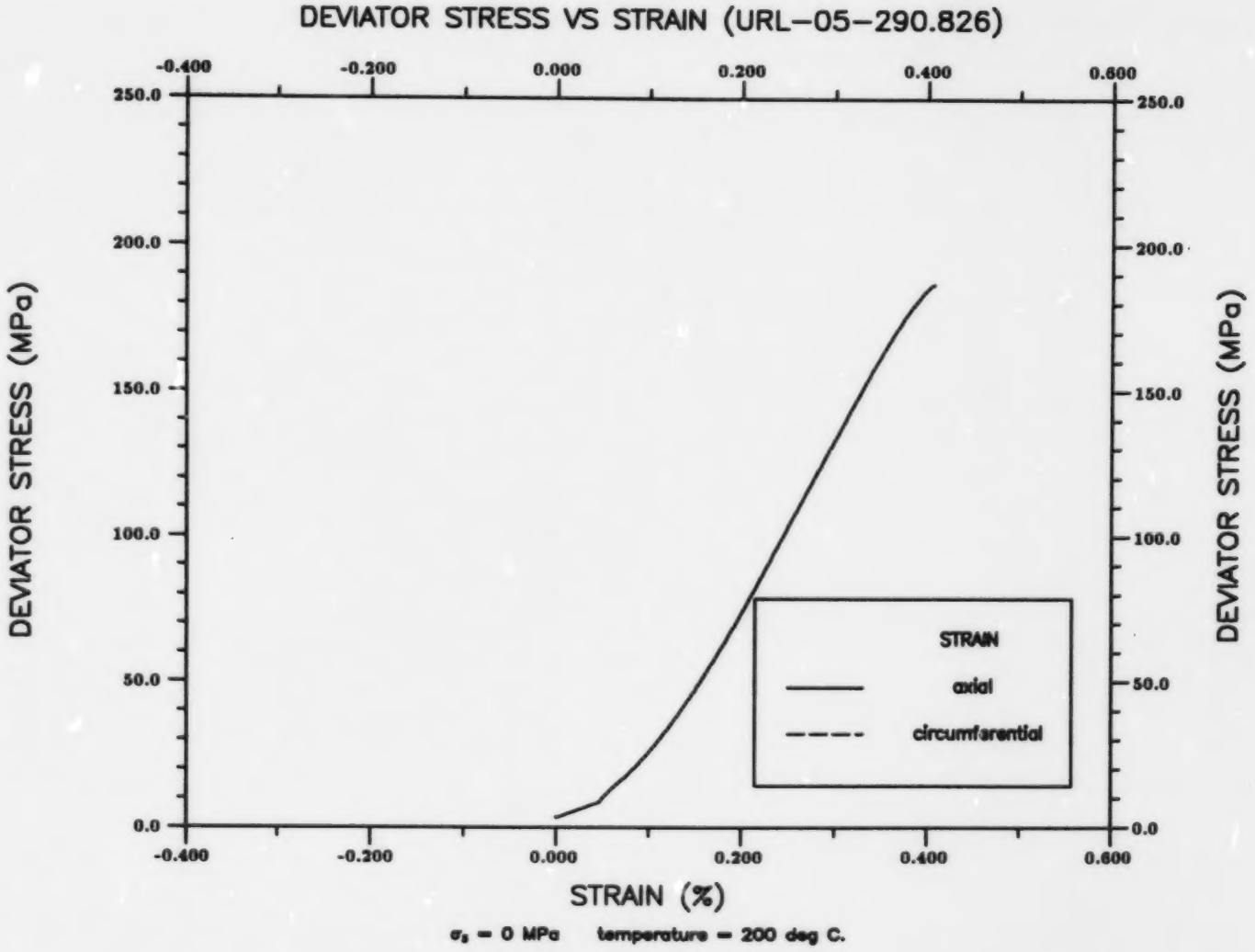

Figure A7. Stress-strain curves for Specimen URL05-290.826 tested at 200° C under the unconfined condition.

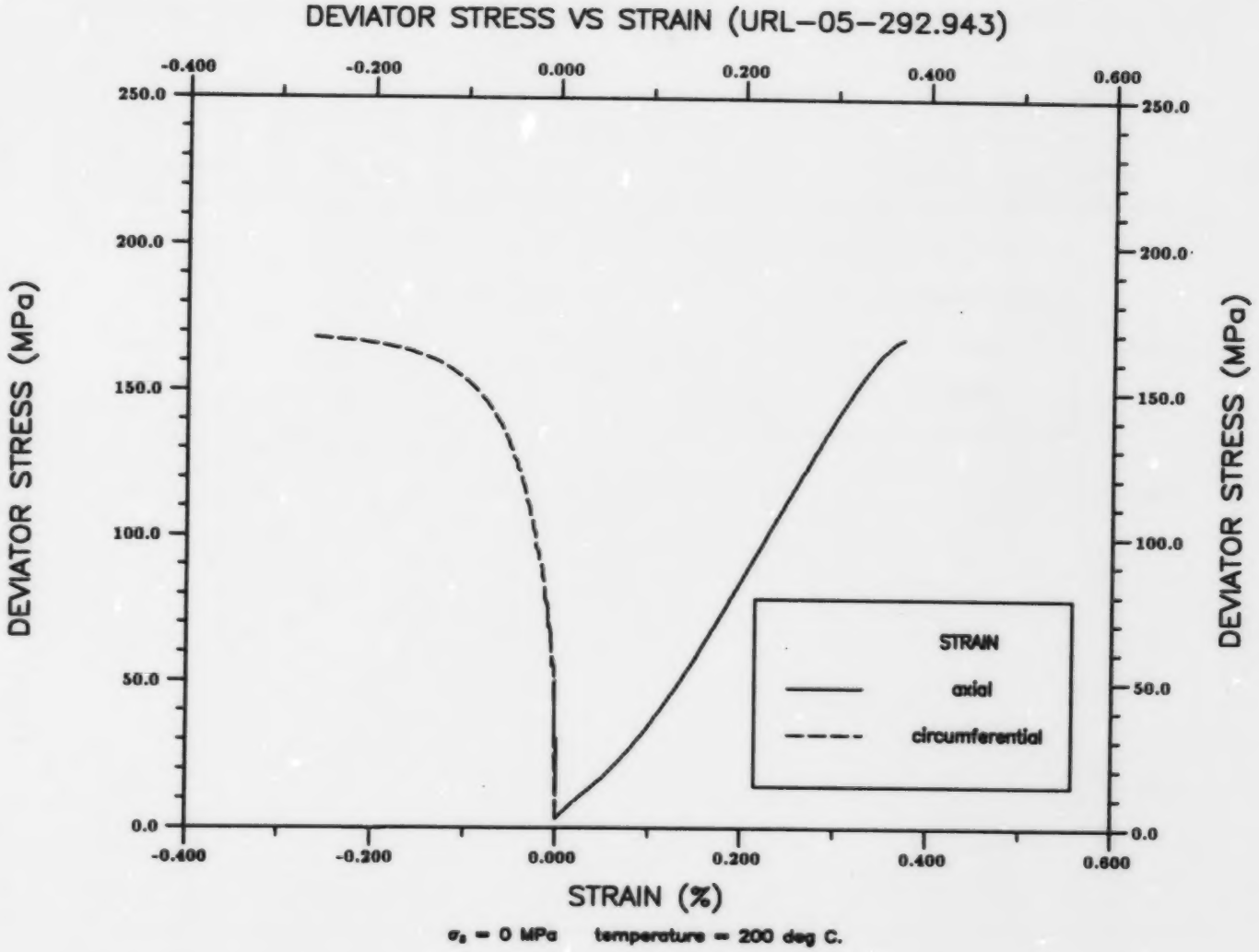

Figure A8. Stress-strain curves for Specimen URL05-292.943 tested at 200° C under the unconfined condition.

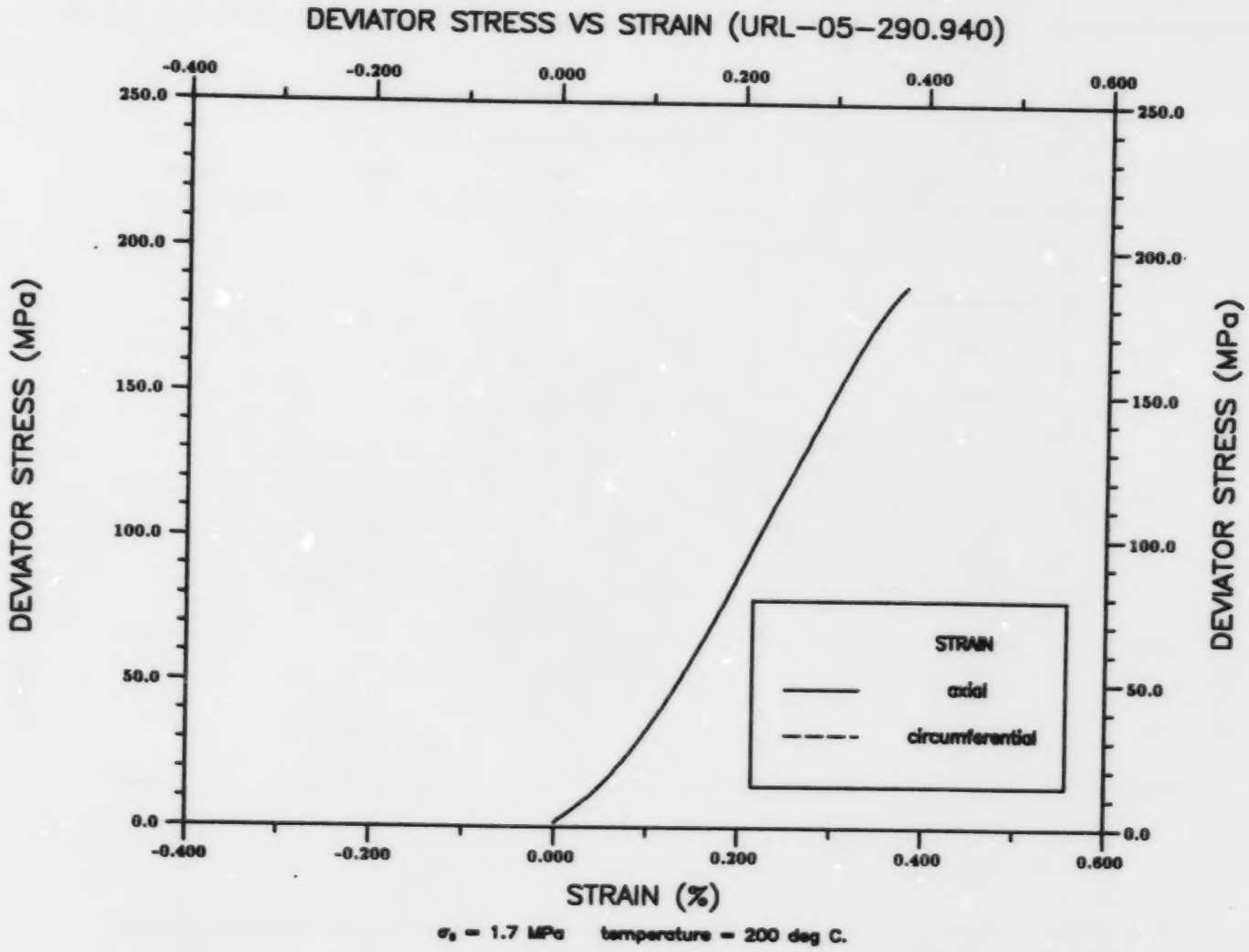

Figure A9. Stress-strain curves for Specimen URL05-290.940 tested at 21° C and at $\sigma_3 = 1.7$ MPa.

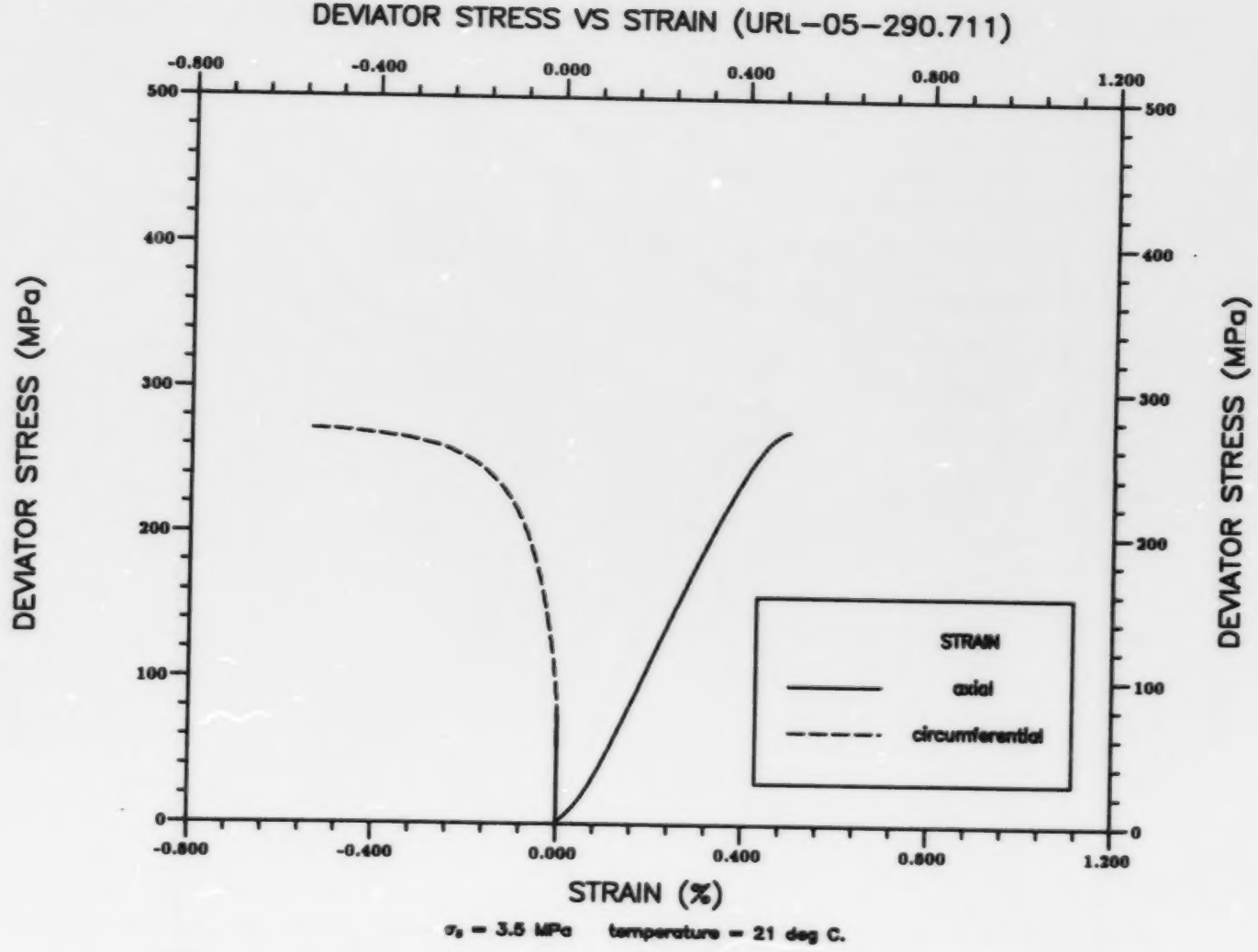

Figure A10. Stress-strain curves for Specimen URL05-290.711 tested at 21° C and at $\sigma_3 = 3.5$ MPa.

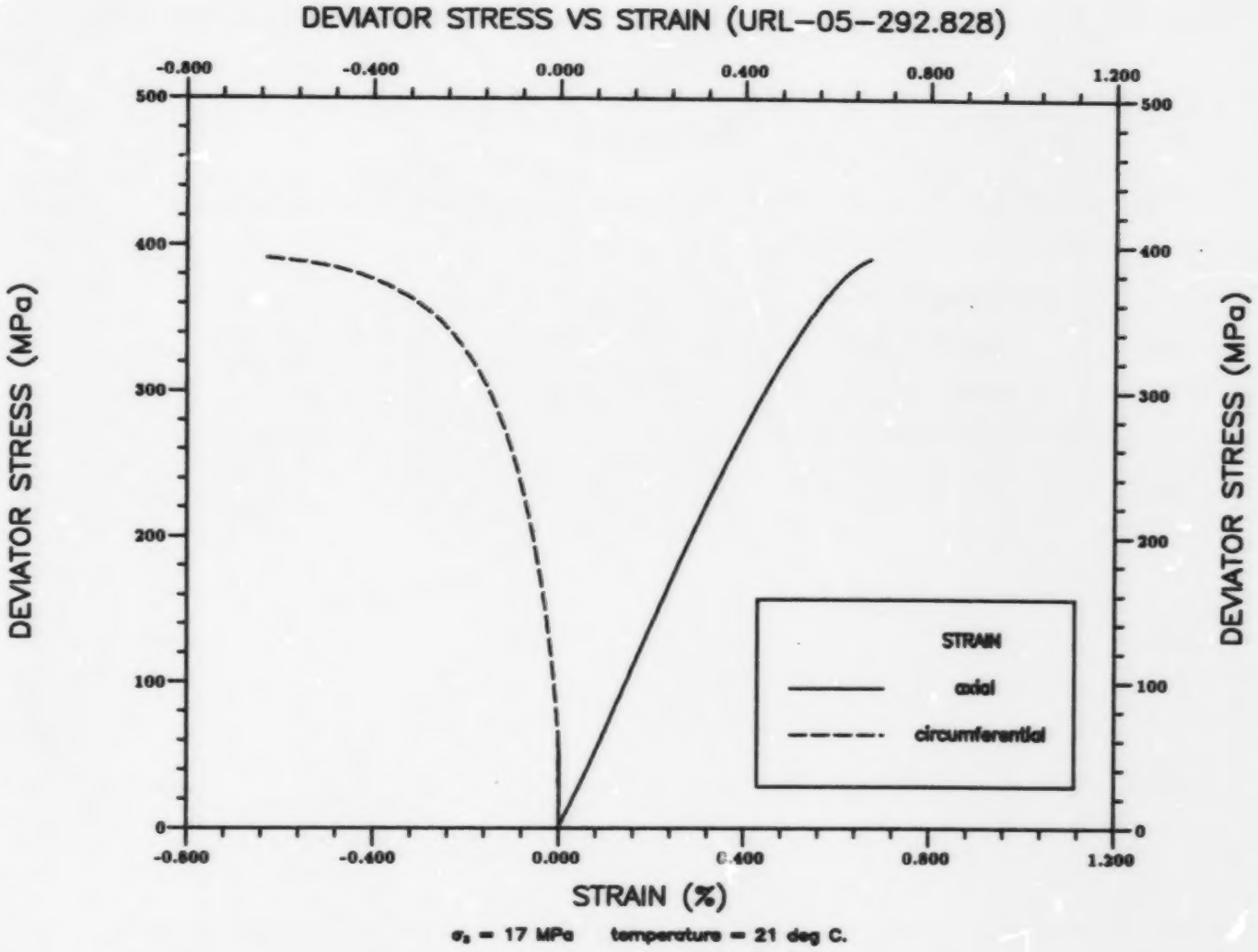

Figure A11. Stress-strain curves for Specimen URL05-292.828 tested at 21° C and at $\sigma_3 = 17$ MPa.

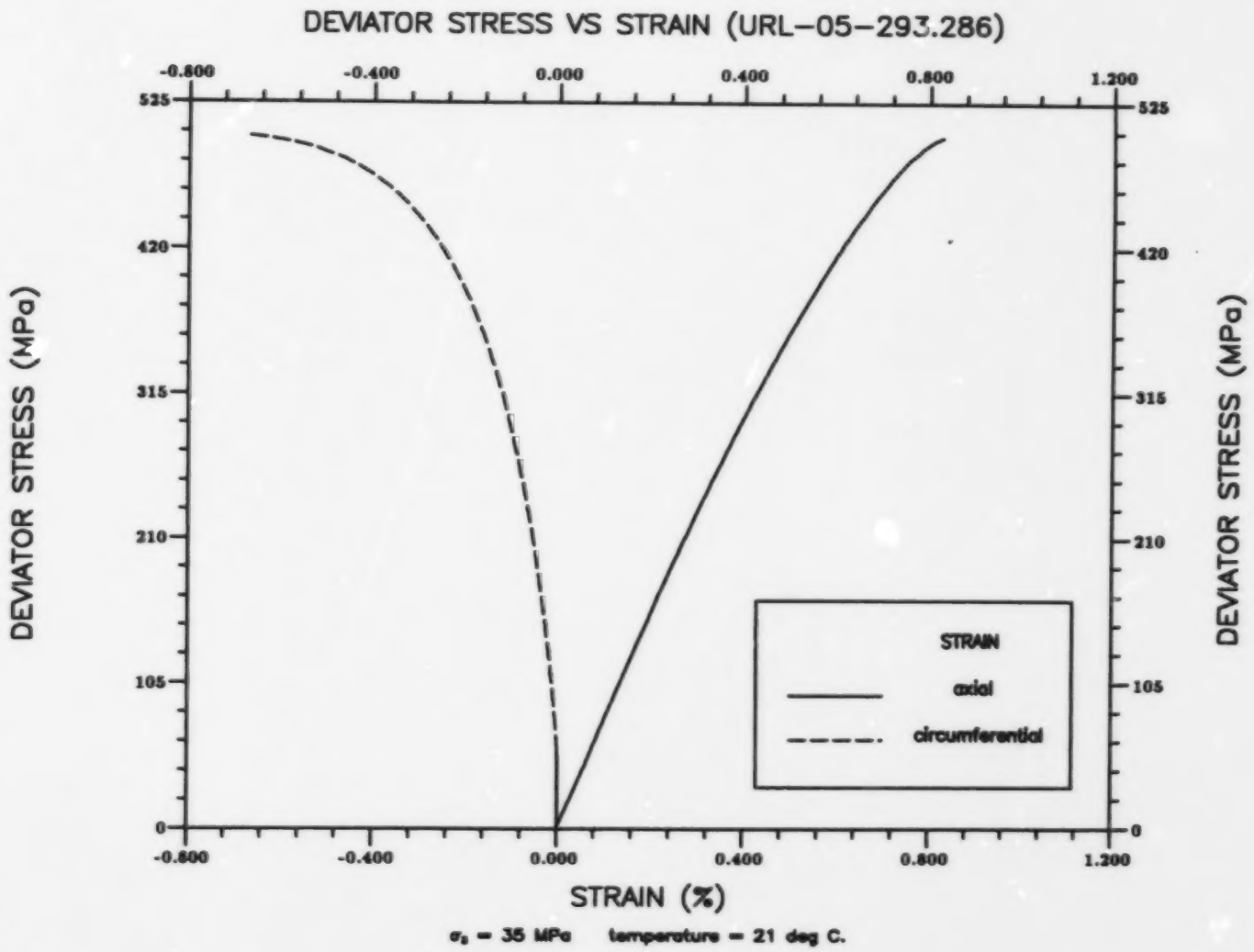

Figure A12. Stress-strain curves for Specimen URL05-293.286 tested at 21° C and at $\sigma_3 = 35$ MPa.